This is a repository copy of *Heterogeneous Nitrate Production Mechanisms in Intense Haze Events in the North China Plain*.

White Rose Research Online URL for this paper:
https://eprints.whiterose.ac.uk/173866/

Version: Accepted Version

Article:

1 **Heterogeneous nitrate production mechanisms in intense haze events in the North**
2 **China Plain**

3

4 **Yuk-Chun Chan[1], Mathew J. Evans[2,3], Pengzhen He[4], Christopher D. Holmes[5], Lyatt**
5 **Jaeglé[1], Prasad Kasibhatla[6], Xue-Yan Liu[7], Tomás Sherwen[2,3], Joel A. Thornton[1], Xuan**
6 **Wang[8], Zhouqing Xie[9], Shuting Zhai[1], and Becky Alexander[1]**

7 [1]Department of Atmospheric Sciences, University of Washington, Seattle, WA 98195, USA

8 [2]National Centre for Atmospheric Science, University of York, York, YO10 5DD, UK

9 [3]Wolfson Atmospheric Chemistry Laboratories, Department of Chemistry, University of York,
10 York, YO10 5DD, UK

11 [4]School of Environment and Tourism, West Anhui University, Lu'an, Anhui 237012, China

12 [5]Department of Earth, Ocean and Atmospheric Science, Florida State University, Tallahassee,
13 FL 32306, USA

14 [6]Nicholas School of the Environment, Duke University, Durham, NC 27708, USA

15 [7]School of Earth System Science, Tianjin University, Tianjin, China

16 [8]School of Energy and Environment, City University of Hong Kong, Hong Kong SAR, China

17 [9]Anhui Key Laboratory of Polar Environment and Global Change, Department of Environmental
18 Science and Engineering, University of Science and Technology of China, Hefei, Anhui,
19 230026, China

20

21 Corresponding author: Becky Alexander (beckya@uw.edu)

22

23 **Key Points:**

24 - Wintertime observations of ^{17}O excess of nitrate in Beijing suggest that the
25   heterogeneous chemistry of NO_2 is a weak source of nitrate in intense haze.
26 - Ozone strongly modulates nitrate production during intense wintertime haze events in
27   Beijing via the heterogeneous chemistry of N_2O_5.

28

29 **Abstract**

30 Studies of wintertime air quality in the North China Plain (NCP) show that particulate-nitrate
31 pollution persists despite rapid reduction in NO_x emissions. This intriguing NO_x-nitrate
32 relationship may originate from non-linear nitrate-formation chemistry, but it is unclear which
33 feedback mechanisms dominate in NCP. In this study, we re-interpret the wintertime
34 observations of ^{17}O excess of nitrate ($\Delta^{17}O(NO_3^-)$) in Beijing using the GEOS-Chem (GC)
35 chemical transport model to estimate the importance of various nitrate-production pathways and
36 how their contributions change with the intensity of haze events. We also analyze the
37 relationships between other metrics of NO_y chemistry and $[PM_{2.5}]$ in observations and model
38 simulations. We find that the model on average has a negative bias of -0.9 ‰ and -36% for
39 $\Delta^{17}O(NO_3^-)$ and $[O_{x,major}](\equiv [O_3] + [NO_2] + [p\text{-}NO_3^-])$, respectively, while overestimating the
40 nitrogen oxidation ratio ($[NO_3^-]/([NO_3^-]+ [NO_2])$) by $+0.12$ in intense haze. The discrepancies
41 become larger in more intense haze. We attribute the model biases to an overestimate of NO_2-
42 uptake on aerosols and an underestimate in wintertime O_3 concentrations. Our findings highlight
43 a need to address uncertainties related to heterogeneous chemistry of NO_2 in air-quality models.
44 The combined assessment of observations and model results suggest that N_2O_5 uptake in aerosols
45 and clouds is the dominant nitrate-production pathway in wintertime Beijing, but its rate is
46 limited by ozone under high-NO_x-high-$PM_{2.5}$ conditions. Nitrate production rates may continue
47 to increase as long as $[O_3]$ increases despite reduction in $[NO_x]$, creating a negative feedback that
48 reduces the effectiveness of air pollution mitigation.

49

50 **Plain Language Summary**

51 Nitrate, a major component of particles in urban air, has been identified as an important driver
52 for recent trends in wintertime haze in the North China Plain. While it has long been known that
53 many chemical reactions can convert gas-phase nitrogen oxides into particulate nitrate in the
54 atmosphere, the contribution from different reactions in intense haze remains elusive. Recently,
55 analysis of oxygen stable isotopes (^{16}O, ^{17}O, ^{18}O) in nitrate has become a promising tool for
56 understanding its chemical origins. In this study, we re-examine the isotopic observations of
57 nitrate in wintertime Beijing and compare them with predictions made by an air-quality model.
58 Our analysis of observations suggests that the model likely overestimates nitrate production via
59 the reactions between nitrogen dioxide gas (NO_2) and particles during intense haze events. After
60 removing this nitrate formation pathway in the model, we demonstrate that nitrate production
61 during intense haze events in Beijing is strongly modulated by ozone, a secondary pollutant
62 whose formation is dependent on nitrogen oxides and volatile organic compounds (VOCs).
63 Policies that result in a reduction of ozone concentrations, possibly through reductions in VOC
64 emissions, will also reduce the formation of nitrate during wintertime haze events.

1 Introduction

Haze events, which are episodes of high concentrations of particulate matter (PM) in the lower troposphere, are common in many metropolitan areas around the world. Industrial activities, heavy traffic, and weak ventilation all favor the occurrence of haze events near population centers. The North China Plain, in particular, has been affected by intense wintertime haze in recent decades (An et al., 2019; Y.-L. Zhang & Cao, 2015). Frequent outbreaks of haze events can lead to short-term surges in premature mortality and long-term reduction in life expectancy (Y. Chen et al., 2013; Lelieveld et al., 2015; C. Song et al., 2017). An important source of fine-mode PM ($PM_{2.5}$, particulate matter with an aerodynamic diameter of equal to or less than 2.5 µm) during haze events is chemical reactions that oxidize gas-phase pollutants into $PM_{2.5}$. To mitigate haze events in metropolitan areas effectively, we must understand the chemical mechanisms driving this secondary production of $PM_{2.5}$.

Nitrate is becoming the dominant inorganic component of $PM_{2.5}$ over China in recent years, especially during wintertime haze events (Fu et al., 2020; Itahashi et al., 2018; H. Li et al., 2019; Y. Sun et al., 2020; Xu et al., 2019; Zhou et al., 2019). The Chinese government implemented a series of clean air policies since the year 2010 that imposed stricter controls on the emissions of SO_2, NO_x ($NO+NO_2$), and primary PM (Zheng et al., 2018). As a result, wintertime sulfate concentration decreased substantially by about 60% from 2014 to 2017 (H. Li et al., 2019; Zhou et al., 2019). A similar long-term concentration reduction was not observed in particulate nitrate (p-NO_3^-) despite a steady decline in NO_x emission in the 2010s (Fu et al., 2020; Itahashi et al., 2018; H. Li et al., 2019; Xu et al., 2019). Analysis of the aerosol sampled in Beijing in 2017 showed that nitrate contributes 25-35% to fine-mode-PM mass during wintertime haze events (H. Li et al., 2019; Xu et al., 2019), which is higher than similar observations in 2014 (<20%) (H. Li et al., 2019). In the eastern US and northern China, the concentration of wintertime secondary aerosol, including nitrate and sulfate, also responds weakly to the reduction of NO_x and SO_2 emissions, which is largely attributed to non-linear chemical feedbacks (Huang et al., 2021; Le et al., 2020; Leung et al., 2020; Shah et al., 2018; Y. Sun et al., 2020). In light of the emerging importance of nitrate in PM pollution in the North China Plain, it is essential to understand the chemistry of nitrate production during wintertime haze events in order to implement effective air pollution mitigation strategies.

Reactions of reactive nitrogen oxides ($NO_y \equiv NO_x + NO_3 + 2\times$dinitrogen pentoxide ($N_2O_5$) + nitryl chloride ($ClNO_2$) + gas-phase nitric acid (HNO_3) + particulate nitrate (p-NO_3^-) + nitrous acid (HONO) + halogen nitrates (ξNO_3, where ξ = Br, Cl, or I) + peroxynitric acid (HNO_4) + peroxyacylnitrates (PANs) + other organic nitrates ($RONO_2$)) control both nitrate production and oxidant budgets in the North China Plain (See Figure 1 and Table S1). Production of NO_3^- (total nitrate $NO_3^- = HNO_3 + $ p-NO_3^-) is the main sink of NO_x in polluted urban air (Kenagy et al., 2018; Shah et al., 2020). In Beijing, the majority of locally produced HNO_3 quickly converts into p-NO_3^- via thermodynamically controlled gas-particle partitioning (Ding et al., 2019). The dominant chemical pathway for nitrate production varies diurnally and seasonally. During the daytime, the oxidation of NO_2 by hydroxyl radical (OH) (Figure 1b, R4) dominates nitrate production, whereas the reactions of nitrate radical (NO_3) (Figure 1b, R8-12), including N_2O_5 uptake (Figure 1b, R10-11), dominate at night (Alexander et al., 2020). Shah et al. (2020) showed that N_2O_5 uptake and OH oxidation contribute similarly to NO_x loss (33% vs. 43% in

111   2017) over summertime in central-eastern China, which is similar to the global annual average
112   (41-42% vs. 28-41%) (Alexander et al., 2020). In winter, on the contrary, N_2O_5 uptake dominates
113   over OH oxidation (51% vs. 23%) (Shah et al., 2020). The conversion of NO_x to NO_3^- is coupled
114   to many other reactive species in the atmosphere, including ozone, peroxy radicals (RO_2), and
115   HONO. For instance, the production of NO_3 radical requires ozone (Figure 1b, R6); yet the
116   efficiency of ozone production is, in turn, controlled by the amount of NO_x and peroxy radicals.
117   Meanwhile, the uptake of NO_2 on aerosols (Figure 1b, R5) and photolysis of p-NO_3^- can produce
118   HONO, which yields OH readily upon photolysis and may control the tropospheric oxidizing
119   capacity during haze events (L. Li et al., 2018; Z. Tan et al., 2019; J. Zhang et al., 2019). A
120   comprehensive representation of nitrate chemistry in models is necessary for accurate predictions
121   of air quality in winter.
122
123   While heterogeneous chemistry (i.e., multi-phase reactions) of NO_y is critical to wintertime
124   nitrate production in urban air, its complexity represents a major source of uncertainty in many
125   air-quality models. The uptake of NO_2 on aerosols, which has been presumed to be a sink of NO_x
126   and a source of NO_3^- and HONO in models, was re-examined in recent modeling studies.
127   Holmes et al. (2019) decreased the uptake coefficients of NO_2 ($\gamma(NO_2)$) in their model after
128   considering the lower estimates of $\gamma(NO_2)$ reported in more recent laboratory studies. Jaeglé et
129   al. (2018) showed that changing the HONO yield of NO_2 uptake to 100% (no HNO_3 formation)
130   improves the simulation of NO_y chemistry over wintertime Northeast United States. A global
131   model study by Alexander et al. (2020) demonstrated that NO_2 uptake has the largest potential
132   influence over the North China Plain. For N_2O_5 uptake on aerosol, the efficiency of nitrate
133   formation is sensitive to the chemical composition (e.g., [Cl^-], [p-NO_3^-], and thickness of
134   organic coating), pH, and water content of aerosols (Bertram & Thornton, 2009; Gaston et al.,
135   2014; Tham et al., 2016; Xia et al., 2019; Zhou et al., 2018). Laboratory-based predictions of the
136   uptake coefficient of N_2O_5 ($\gamma(N_2O_5)$) on aerosols often differ from the observation-based
137   estimates by orders of magnitudes (e.g., McDuffie et al., 2018; C. Yu et al., 2020). In addition to
138   reactions on aerosol surfaces, recent modeling studies also suggest that uptake of NO_y in cloud
139   droplets is an overlooked sink of NO_x (Holmes et al., 2019). Cloud uptake of NO_y contributes up
140   to 25% NO_x loss at higher latitudes annually (Alexander et al., 2020; Holmes et al., 2019). Given
141   the large number of remaining uncertainties in heterogeneous chemistry of NO_y, models need
142   additional observational constraints for improving the representation of these chemical processes
143   in air quality models.
144
145   The oxygen isotopic composition of nitrate provides an independent piece of information related
146   to the formation of nitrate. In particular, ^{17}O excess ($\Delta^{17}O$) in nitrate, which is determined solely
147   by the relative importance of ozone to other oxidants during the oxidation of the members of
148   NO_y family (Michalski et al., 2003), has proven to be a promising proxy for quantifying nitrate-
149   production mechanisms in various environmental contexts (e.g., Alexander et al., 2020; Geng et
150   al., 2017; Savarino et al., 2013). Shao et al. (2019) analyzed observations of $\Delta^{17}O(SO_4^{2-})$ in
151   wintertime Beijing and demonstrated the importance of heterogeneous chemistry for sulfate
152   formation during haze events. For $\Delta^{17}O(NO_3^-)$, three previous studies have reported observations
153   in the North China Plain during winter haze events (He et al., 2018; W. Song et al., 2020; Y.
154   Wang et al., 2019). Their analyses of the observations suggested that uptake of N_2O_5 and the
155   oxidation of volatile organic compounds (VOCs) by NO_3 radicals (Figure 1b, R12) dominate
156   wintertime nitrate production near Beijing. However, their interpretation of the observations

157   relies on highly simplified models of nitrate production and several assumptions about the

158   concentration of radicals in urban air. In this study, we use a 3-D chemical transport model with

159   coupled HO_x-NO_x-VOC-ozone-halogen-aerosol tropospheric chemistry to re-interpret the

160   observations of $\Delta^{17}O(NO_3^-)$ in the North China Plain in order to gain insight into the

161   mechanisms of NO_y chemistry during winter haze events.
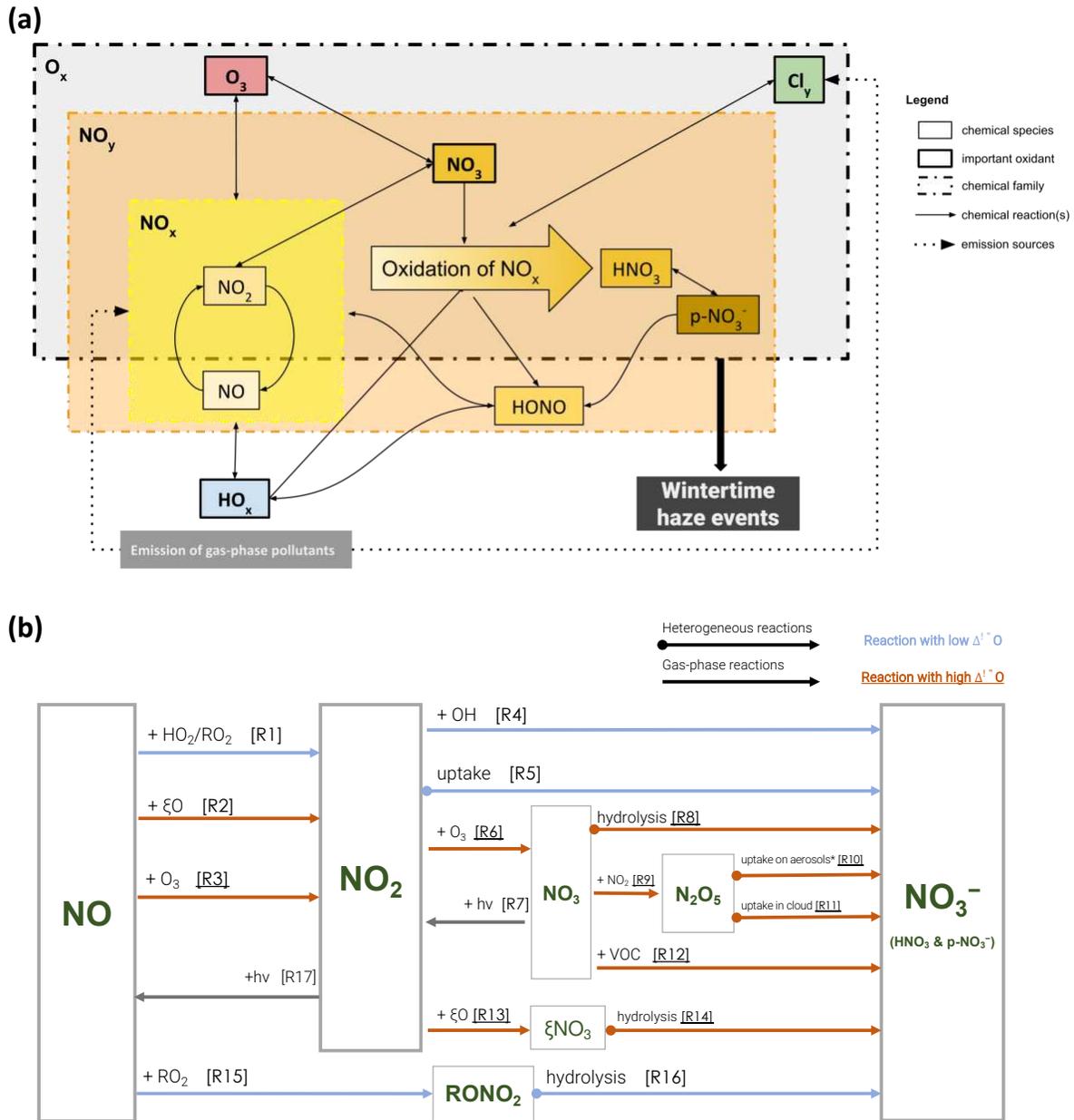
162

163

(a)

(b)

Figure 1. Simplified schematic of the chemistry of nitrate production in urban air. 1(a) is the schematic of the coupling of nitrate production and the emission of gas-phase pollutants, the NO_y chemical family, the budget of odd oxygen species, and PM pollution. 1(b) is the schematic of nitrate production pathways in the model and important intermediate species from the oxidation of NO_x to NO_3^- ($[NO_3^-] = [HNO_3] + [p\text{-}NO_3^-]$). "$\xi$" stands for the

halogens (Cl/ Br/I), while "VOC" stands for volatile organic compounds. N_2O_5 uptake on aerosols (R10) can undergo two possible pathways, depending on the chloride content in the aerosol. The chemical equation and other details of the reactions R1 to R17 can be found in Table S1.

164

165   **2 Data and Methods**

166

167   **2.1 Measurements of $\Delta^{17}O(NO_3^-)$, aerosol, and trace gases during Beijing in winter 2014-15**

168

169   Observations of $\Delta^{17}O(NO_3^-)$ in Beijing were previously published in He et al. (2018), Y. Wang et
170   al. (2019), and W. Song et al. (2020) and are briefly described here. Most of the aerosol samples
171   were collected in the Beijing metropolitan area from October 2014 to January 2015 and later sent
172   to IsoLab at the University of Washington for isotopic analysis. The location of the measurement
173   sites is shown in Figure S1(a). He et al. (2018) and W. Song et al. (2020) used collection
174   intervals of about 12 hours for each aerosol sample, whereas Y. Wang et al. (2019) used 23 hours.
175   The aerosol filters collected both HNO_3 and p-NO_3^-, so the observed $\Delta^{17}O(NO_3^-)$ contains $\Delta^{17}O$
176   signals from both species (He et al., 2018). We compute the daily mean of $\Delta^{17}O(NO_3^-)$ from
177   these published measurements and obtain a dataset with 51 data points between 1 October 2014
178   and 15 January 2015.

179

180   To evaluate the modeled concentration of $PM_{2.5}$, p-NO_3^-, NO_2, and ozone in Beijing, we use
181   measurements of these species reported in He et al. (2018), Y. Wang et al. (2019), and W. Song et
182   al. (2020). We also consider similar measurements at other Beijing air-quality stations that are
183   operated by the China Ministry of Ecology and Environment as a complementary dataset
184   (location of these sites are shown in Figure S1(a)). These air-quality measurements are publicly
185   available on https://quotsoft.net/air (last accessed on 26 January 2021).

186

187

188   **2.2 GEOS-Chem 3-D Chemical Transport Model simulations**

189

190   We use the three-dimensional global chemical transport model GEOS-Chem (version 12.7.0;
191   hereafter GC) to simulate the evolution of haze events in winter 2014-15. This version of the GC
192   model code is accessible from https://doi.org/10.5281/zenodo.3634864 (last accessed on 26
193   January 2021). The model considers detailed HO_x-NO_x-VOC-ozone-halogen-aerosol chemistry
194   in the troposphere (Fisher et al., 2018; Kasibhatla et al., 2018; Sherwen et al., 2017; X. Wang et
195   al., 2019, 2020). The Fast-JX module in GC calculates aerosol radiative effects and photolysis
196   rates (Eastham et al., 2014; Neu et al., 2007). The partitioning between the HNO_3 and p-NO_3^- is
197   determined by an aerosol thermodynamic equilibrium module ISORROPIA II (Fountoukis &
198   Nenes, 2007). The deposition schemes for trace gases and aerosols in GC are described in Y.
199   Wang et al. (1998), H. Liu et al. (2001), L. Zhang et al. (2001), and Jaeglé et al. (2018). Since
200   GC uses offline meteorological data to drive simulations by design, it will not be able to capture
201   the feedback processes involving aerosol-boundary interaction, which can potentially be
202   important during haze events in wintertime East China (Huang et al., 2020). Earlier versions of
203   GC have also been used to investigate NO_x and PM pollution in metropolitan areas (e.g., Jaeglé
204   et al., 2018; Shah et al., 2020).

205

206   The NO_y chemistry in GC has been updated substantially in recent versions of the model.
207   Holmes et al. (2019) modified the uptake coefficients for NO_2, NO_3, and N_2O_5 on different
208   aerosols based on recent laboratory studies. In particular, $\gamma(NO_2)$ on sulfate-nitrate-ammonium
209   (SNA) aerosol has been set to 5×10^{-6}, which is a factor-of-20 reduction compared to the
210   previous work. The latest versions of GC also incorporated the uptake of NO_2, NO_3 and N_2O_5 in

211   cloud droplets, following the entrainment-limited scheme described in Holmes et al. (2019) for
212   partly cloudy conditions. For the uptake of N_2O_5 on SNA aerosol, the latest version of GC now
213   considers the inhibiting effects of organic coating through the parametrization described in
214   McDuffie et al. (2018), which was built on top of the Bertram and Thornton (2009) scheme to
215   calculate the reaction probability of N_2O_5 on aerosol. Particulate-nitrate photolysis described in
216   Kasibhatla et al. (2018) is currently an optional feature in GC and is switched off by default. For
217   gas-phase NO_y chemistry, the latest updates include the reactions of C1-C3 alkyl nitrate, as
218   described in Fisher et al. (2018). While the previous studies independently showed that these
219   chemistry updates improved the representation of NO_y in the model, no study to date has yet
220   examined the combined effects of these updates on model simulations of wintertime haze events
221   in China.
222
223   In this study, we use version 12.7.0 of GC as our "base model". Driven by GEOS-FP
224   meteorological data assimilation products with a native horizontal resolution of 0.25° x 0.3125°
225   and 72 vertical levels, the base simulation was run at a coarser spatial resolution (4° latitude x 5°
226   longitude and 47 vertical levels) to attain global coverage. We also performed nested-grid
227   regional simulations for East Asia at a higher horizontal resolution (0.25° latitude x 0.3125°
228   longitude) by using output from the corresponding global simulations as boundary conditions
229   (See Figure S1(b) and S1(c) for grid size and boundaries). The model simulates the mixing of
230   chemical species in the planetary boundary layer using the non-local mixing scheme from Lin
231   and McElroy (2010). Anthropogenic emissions of reactive gases and aerosols over the United
232   States, Canada, Asia, and Africa are from the regional emissions inventories EPA/NEI2011,
233   APEI, MIX, and DICE-Africa, respectively (M. Li et al., 2017; Marais & Wiedinmyer, 2016).
234   NO_x emissions from MEIC (the emission inventory for China in MIX framework) between 2005
235   and 2018 have recently been validated by the satellite retrievals of NO_2 columns in Shah et al.
236   (2020) and showed a good agreement. Emissions in the rest of the world are from the
237   Community Emissions Data System (CEDS) inventory (Hoesly et al., 2018). Biomass burning
238   emissions are from the Global Fire Emissions Database (GFED 4.1s) (van der Werf et al., 2017).
239   Lightning-NO_x emissions in the model are estimated based on a satellite lightning climatology
240   described in Murray et al. (2012). Soil-NO_x emissions are estimated offline using the algorithm
241   described in Hudman et al. (2012). The model simulation period is from August 2014 to January
242   2015, in which the first two months are used for "spinning-up" the model. To address the
243   uncertainty in NO_y chemistry, we conduct a series of model sensitivity experiments at 4° latitude
244   x 5° longitude resolution. The detailed configurations for these simulations are described in
245   Section 3.2.2 and Text S2 in SI.
246
247
248   **2.3 Calculation of $\Delta^{17}O(NO_3^-)$ in model simulations**
249
250   Following the approach of Alexander et al. (2020), we use local chemical production rates to
251   calculate $\Delta^{17}O(NO_3^-)$, by which we assume that $\Delta^{17}O(NO_3^-)$ is controlled by local NO_x cycling
252   and nitrate production (See Figure S2). This method works well for intense haze events in
253   wintertime North China Plain, where most NO_3^- is produced locally over the North China Plain
254   (See Figure S3). The $\Delta^{17}O$ in tropospheric ozone ($\Delta^{17}O(O_3)$) is assumed to be 26‰ based on
255   recent measurements (Vicars & Savarino, 2014). We assume that only the terminal oxygen atom
256   of ozone is transferred during oxidation reactions; hence the $\Delta^{17}O$ value of the oxygen atom

257 transferred is equal to 39‰ ($= \frac{3}{2} \times 26‰$, denoted as $\Delta^{17}O(O_3^*)$) (Morin et al., 2011). For

258 calculation of $\Delta^{17}O(NO_2)$, we assume isotopic equilibration during the daytime for all nitrate

259 production pathways. The longer lifetime of NO_x in wintertime North China Plain (≈ 21 to 27

260 hours estimated by Shah et al. (2020)) suggests that NO_x oxidation rates are slow enough to

261 make this a reasonable assumption. Figure S2 also shows the assumed $\Delta^{17}O(NO_3^-)$ values for

262 each nitrate formation pathway in the model.

263

264

265 **2.4 Other metrics for evaluating NO_y chemistry**

266

267 In addition to $\Delta^{17}O$, we also use the concentration and speciation of the odd oxygen family (O_x)

268 to evaluate the performance of the model in simulating NO_y chemistry. In theory, O_x includes all

269 the chemical species that cycle with ozone and atomic oxygen in the atmosphere via

270 photochemical reactions and is highly coupled with the local nitrate production (Bates & Jacob,

271 2020; Lu et al., 2019; Womack et al., 2019).

272

273 Here, we define total O_x as the weighted sum of ozone and other species that cycle with ozone

274 and atomic oxygen in the model:

275

276
$$O_x \equiv O_3 + NO_2 + 2NO_3 + 3N_2O_5 + HNO_3 + p\text{-}NO_3^- + PANs + RONO_2 + HNO_4 + \xi O$$

277
$$+ \xi NO_2 + 2\xi NO_3 + \sum_{n=2}^{5} n\xi_2O_n + 2O\xi O$$

278

279 where $\xi = Br$, Cl, or I. Our definition of O_x is very similar to the one used in Bates and Jacob

280 (2020), except that we (1) include p-NO_3^- and (2) exclude the short-lived radical species (e.g.,

281 $O(^1D)$ and Criegee intermediates) that have a negligible impact on total O_x abundances. We

282 consider p-NO_3^- to be an O_x member because of the rapid equilibrium partitioning between

283 HNO_3 and p-NO_3^- on fine-model aerosol and the potential importance of renoxification in urban

284 air from the photolysis of p-NO_3^- (Bao et al., 2018; Kasibhatla et al., 2018; Y. Liu et al., 2019;

285 Ye et al., 2017). Womack et al. (2019) also included p-NO_3^- in their definition of generalized

286 odd oxygen family. While GC can simulate and output all the species listed in our definition of

287 O_x, most of the measurements in Beijing only include the concentration of O_3, NO_2, and p-NO_3^-

288 (with possible interference of HNO_3, as explained in Section 2.1). The incomplete observations

289 of O_x only have minor effects on our model-observation comparison because O_3, NO_2, and p-

290 NO_3^- are the dominant (>95%) O_x species in wintertime Beijing in the model (See more detailed

291 analysis in Section 3.1). We denote the sum of O_3, NO_2, and p-NO_3^- as $O_{x,major}$.

292

293 Since the speciation of O_x is sensitive to NO_y chemistry, we also compare the ratio of different

294 O_x species in the observations and the model simulations. In particular, we compute the nitrogen

295 oxidation ratio (NOR) using the mixing ratios of NO_2 and NO_3^-:

296

297
$$NOR \equiv \frac{[NO_3^-]}{[NO_3^-] + [NO_2]} = \frac{[p\text{-}NO_3^-] + [HNO_3]}{[p\text{-}NO_3^-] + [HNO_3] + [NO_2]}$$

298

299 NOR ranges from 0 (complete absence of NO_3^-) to 1 (complete oxidation of all NO_2). This
300 dimensionless ratio indicates the efficiency of the oxidation of NO_x and is less prone to absolute
301 errors in simulating NO_x concentrations (such as uncertainties in emissions). NOR has been
302 widely used in the analysis of nitrate formation mechanisms in other studies (e.g., He et al.,
303 2018; P. Liu et al., 2020; Shi et al., 2019; Xu et al., 2019).
304
305
306 **2.5 Haze-regime categorization**
307
308 To facilitate our analysis of the relationships between the chemistry metrics and the intensity of
309 haze events, we categorize the data into four haze regimes according to the surface $PM_{2.5}$
310 concentration: "light haze" ($[PM_{2.5}] \leq 75$ µg m^{-3}), "moderate haze" events (75 µg m^{-3} <$[PM_{2.5}] \leq$
311 150 µg m^{-3}), "severe haze" events (150 µg m^{-3} <$[PM_{2.5}] \leq 225$ µg m^{-3}), and "extreme haze"
312 events ($[PM_{2.5}] > 225$ µg m^{-3}) (See Table S2 for the frequency of different haze regimes). For
313 the observations, we compute the average of daily mean $[PM_{2.5}]$ observed at the Beijing air-
314 quality stations (both urban and suburban stations, 22 stations in total) to determine the haze
315 regime of a particular day. The inter-station average $[PM_{2.5}]$ can better reflect the intensity of
316 regional haze events than the single-station measurements. For model data, we use the modeled,
317 mean surface $[PM_{2.5}]$ over the Beijing gridbox in coarse-resolution simulations. It is noted that
318 the choice of this categorization does not imply the existence of statistically significant
319 differences between chemical metrics in different haze regimes or abrupt shifts in NO_y chemistry
320 at regime boundaries (where $[PM_{2.5}] = 75$, 150, or 225 µg m^{-3}). Instead, this categorization is
321 merely used for illustrating and communicating some general trends in NO_y chemistry as haze
322 intensifies. Similar categorizations have also been adopted in other studies of nitrate pollution in
323 Beijing (e.g., Fu et al., 2020; He et al., 2018; P. Liu et al., 2020). When we are referring to
324 patterns that are seen across multiple haze regime, the terms "intense haze" ($[PM_{2.5}] > 75$ µg m^{-3})
325 and "more intense haze" ($[PM_{2.5}] > 150$ µg m^{-3}) are sometimes used.
326
327
328 **3 Results**
329
330 **3.1 Observations of $\Delta^{17}O(NO_3^-)$ in Beijing**
331
332 A compilation of all available $\Delta^{17}O(NO_3^-)$ observations reveals a positive relationship between
333 $\Delta^{17}O(NO_3^-)$ and $PM_{2.5}$ concentration in Beijing during winter 2014-15 (Figure 2). The median of
334 $\Delta^{17}O(NO_3^-)$ increases from 26.1‰ in light haze to 31.5‰ in extreme haze (Figure 2b). Similar
335 positive relationships between $\Delta^{17}O(NO_3^-)$ and $[PM_{2.5}]$ have also been reported in He et al.
336 (2018) and Y. Wang et al. (2019). The positive relationship can still be seen when we analyze
337 daytime and nighttime measurements separately (Figure S4). The lack of strong diurnal
338 variability in $\Delta^{17}O(NO_3^-)$ in observations is consistent with the long lifetime of NO_x in
339 wintertime North China Plain shown by previous modeling studies (e.g., Shah et al., 2020). The
340 higher $\Delta^{17}O(NO_3^-)$ measured in intense haze indicates that the relative importance of high-$\Delta^{17}O$
341 pathways involving O_3 increases with $PM_{2.5}$ concentration.
342
343 Figure 2 also shows that the variability of $\Delta^{17}O(NO_3^-)$ is larger on days with lower $[PM_{2.5}]$. The
344 standard deviation (s.d.) of $\Delta^{17}O(NO_3^-)$ decreases from 3.7‰ in light haze to 1.7‰ intense haze.

345   The observed smaller variability of $\Delta^{17}O(NO_3^-)$ in intense haze may be explained by the weaker
346   ventilation and the overwhelming contribution of nitrate from local production (See Figure S3).
347   We also note that very high variability in $\Delta^{17}O(NO_3^-)$ is only seen in the light-haze observations
348   from Y. Wang et al. (2019) (the corresponding s.d. is 3.9‰). Observations in He et al. (2018) and
349   W. Song et al. (2020) show a similar variability in $\Delta^{17}O$ (the overall s.d. are 1.6‰ and 1.4‰,
350   respectively) and do not contain the low $\Delta^{17}O(NO_3^-)$ values (<26‰) reported by Y. Wang et al.
351   (2019). Thus, we focus our analysis more on intense haze when the observations from all three
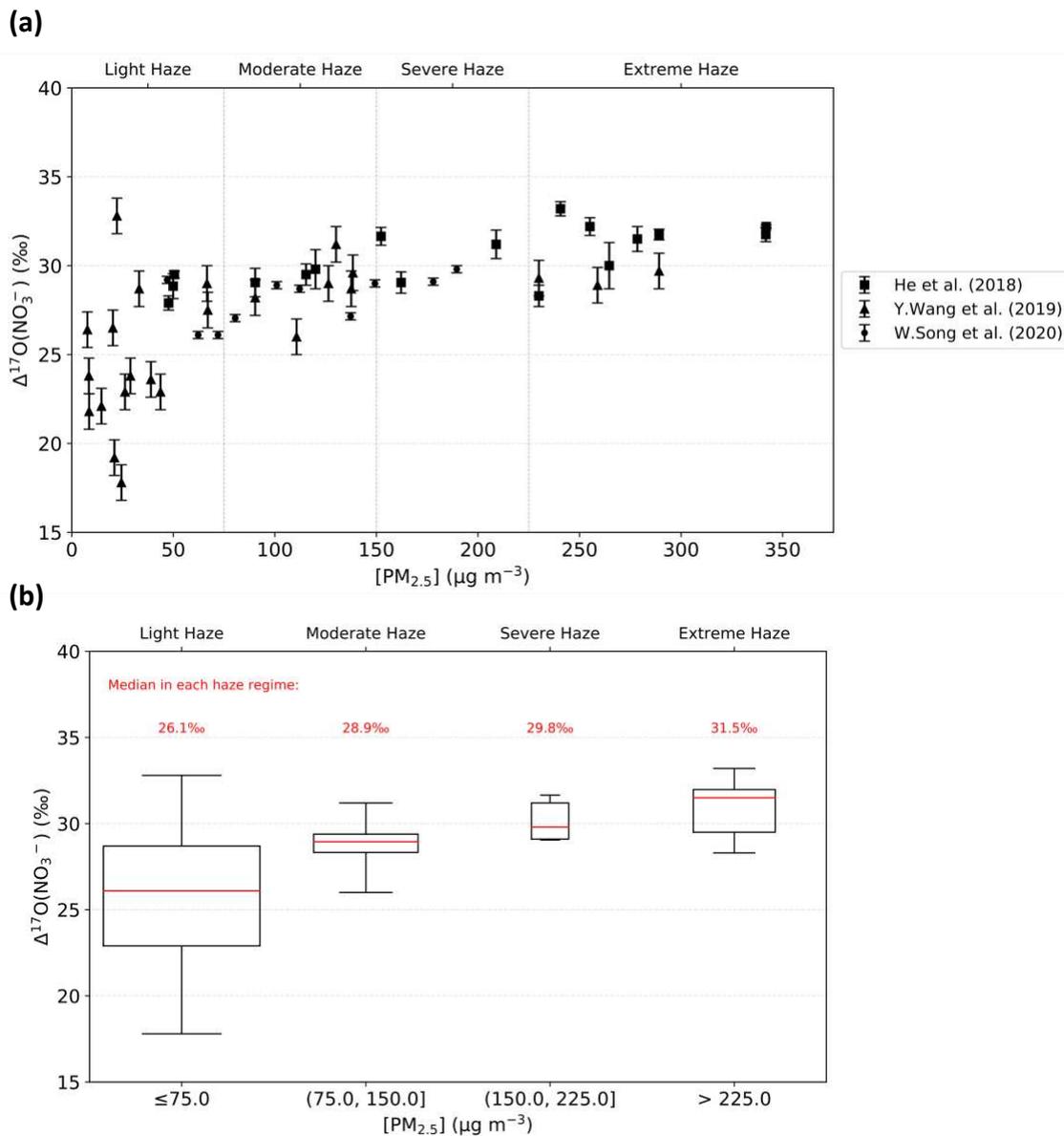352   studies are in better agreement on the magnitude and variability in $\Delta^{17}O(NO_3^-)$.
353

(a)

(b)

Figure 2. Observed relationship between $\Delta^{17}O(NO_3^-)$ and PM$_{2.5}$ concentration. The scatter
plot in 2(a) shows the daily-average measurements in He et al. (2018) (squares), Y. Wang et
al. (2019) (triangles), and W. Song et al. (2020) (circles). The number in red above each
box shows the value of the median of $\Delta^{17}O(NO_3^-)$ in each haze regime. The error bars

represent the $\pm 2\sigma$ standard deviation uncertainty range for the $\Delta^{17}O$ measurements. The box plot in 2(b) shows the statistics of the observed $\Delta^{17}O(NO_3^-)$ in each haze regime. The red line indicates the median; the top and the bottom of the box indicate the 75th percentile and the 25th percentile, respectively; the whiskers indicate the maximum and the minimum. The width of boxes scales with the number of samples in each haze regime.

3.2 Model Results

3.2.1 Base Model

Figure 3 compares the magnitude of modeled and observed $\Delta^{17}O(NO_3^-)$ in Beijing in intense haze. While the modeled median $\Delta^{17}O(NO_3^-)$ in moderate haze (29.5‰) and severe haze (29.1‰) lie within the range of observations, most of the modeled $\Delta^{17}O(NO_3^-)$ in extreme haze (median = 27.3‰) are lower than the minimum value in the observations (28.3‰). The lower $\Delta^{17}O(NO_3^-)$ in extreme haze compared to moderate and severe haze means the base model predicts a negative relationship between $\Delta^{17}O(NO_3^-)$ and $[PM_{2.5}]$ in intense haze (Figure 3), which is the opposite relationship shown in the observations. Modeled median $\Delta^{17}O(NO_3^-)$ in moderate haze is 2.2‰ higher than that in extreme haze. Lower $\Delta^{17}O(NO_3^-)$ in extreme haze cannot be explained by the modeled difference in $\Delta^{17}O(NO_2)$, of which the median changes by less than 0.5‰ across different types of haze events (Figure S5).

The base model also cannot reproduce a sufficient amount of O_x, the observed O_x speciation, nor the observed NOR in Beijing in intense haze (Figure 4 and Figure 5). Modeled $[O_{x, major}]$ in intense haze is 36% lower than the observations on average. The bias in modeled $[O_x]$ in the North China Plain is mainly caused by an underestimate of $[NO_2]$ and $[O_3]$ (Figure 4, and more discussion in Section 4.2). In extreme haze, the base model underestimates the mean of $[NO_2]$ and $[O_3]$ by 55% and 54%, respectively. The large model-observation discrepancy in $[NO_2]$ cannot be explained by the long-known interference of NO_z species (members in the NO_y family that are not NO or NO_2) in chemiluminescence-based measurements (Lamsal et al., 2008; Reed et al., 2016), because both our model (see Figure S6) and other observations suggest that non-NO_3^- gas-phase NO_z species' (e.g., PAN) concentration is small in comparison with $[NO_x]$ in wintertime in Beijing (S. Chen et al., 2020; B. Zhang et al., 2017; G. Zhang et al., 2020; H. Zhang et al., 2014). The underestimate of NO_2 leads to a modeled overestimate of NOR (0.33) in intense haze compared to the observations (0.21). The discrepancy between modeled and observed NOR increases with $[PM_{2.5}]$. In extreme haze, the modeled median NOR (0.50) is higher than the observed maximum (0.47) (Figure 5).

The base model's bias in $\Delta^{17}O(NO_3^-)$, $[O_x]$, and NOR persists even when a higher horizontal spatial resolution is used. The range of the chemical metrics increases with model resolution, but the median and the mean remain largely unchanged (Figures 3, 4 and 5). The relationship between modeled $\Delta^{17}O(NO_3^-)$ and $[PM_{2.5}]$ is still negative in intense haze (Figure 3). Moreover, the extended range of modeled $\Delta^{17}O(NO_3^-)$ still cannot capture the maximum and minimum in observations. A similar model underestimate of mean $[O_x]$ during intense haze events is seen in both the regional-level and the site-level comparison (Figure 4 and Figure S7). The nested-grid simulation predicts a slightly lower median NOR (-0.01, -0.05, and -0.07 in moderate, severe,

395 and extreme haze, respectively), but the modeled NOR is still too high compared to the
396 observations (Figure 5). The comparison between nested-grid and global simulations suggests
397 that low horizontal spatial resolution is not the fundamental cause for the model's bias in NO_y
398 chemistry over the North China Plain. Comparison of observed and modeled mixed layer depths
399 also suggests that the bias in the thickness of vertical mixing layer is not a cause of the model
400 biases in trace gas concentrations (See Figure S8).

402 In the base simulation, the major low-$\Delta^{17}O$ pathways in Beijing are gas-phase oxidation of NO_2
403 by OH and NO_2 uptake on aerosols, which contribute 34.4% and 19.0 % to nitrate production on
404 average over winter 2014-15, respectively (Figure 6). The major high-$\Delta^{17}O$ pathways are N_2O_5
405 uptake on aerosols (33.6%) and clouds (11.3%) (Figure 6). The relative importance of high-$\Delta^{17}O$
406 pathways and low-$\Delta^{17}O$ pathways remains at around a ratio of 1:1 from light haze to severe haze
407 events. In extreme haze, the contribution from NO_2 uptake increases sharply to 35.9% and
408 becomes higher than N_2O_5 uptake on aerosols and clouds (30.0%), resulting in relatively low
409 values of $\Delta^{17}O(NO_3^-)$ (Figure 6).

411 The model-observation comparison of the $\Delta^{17}O(NO_3^-)$ in extreme haze suggests that the standard
412 version of GC either overestimates the contribution of low-$\Delta^{17}O$ pathways and/or underestimates
413 the contribution of high-$\Delta^{17}O$ pathways as $PM_{2.5}$ increases. In the base simulation, the modeled
414 reduction in $\Delta^{17}O(NO_3^-)$ in extreme haze is driven by an increase in NO_2 uptake rate and a
415 decrease in N_2O_5 uptake on aerosols (Figure 6a), suggesting that the modeled rate of NO_2 uptake
416 is too high and/or the rate of N_2O_5 uptake is too low in extreme haze. It is also possible that the
417 model underestimates the contribution of the other high-$\Delta^{17}O$ nitrate production pathways, such
418 as reactions between NO_3 and VOCs (Figure 1b, R12) and the hydrolysis of halogen nitrates
419 (Figure 1b, R14). However, further analysis and model sensitivity simulations suggest that either
420 these reactions are negligible and/or cannot resolve the model biases in the chemical metrics
421 because of the limited supply of NO_3 and N_2O_5 in intense haze (Refer to Text S1 and Text S2.2 in
422 SI).
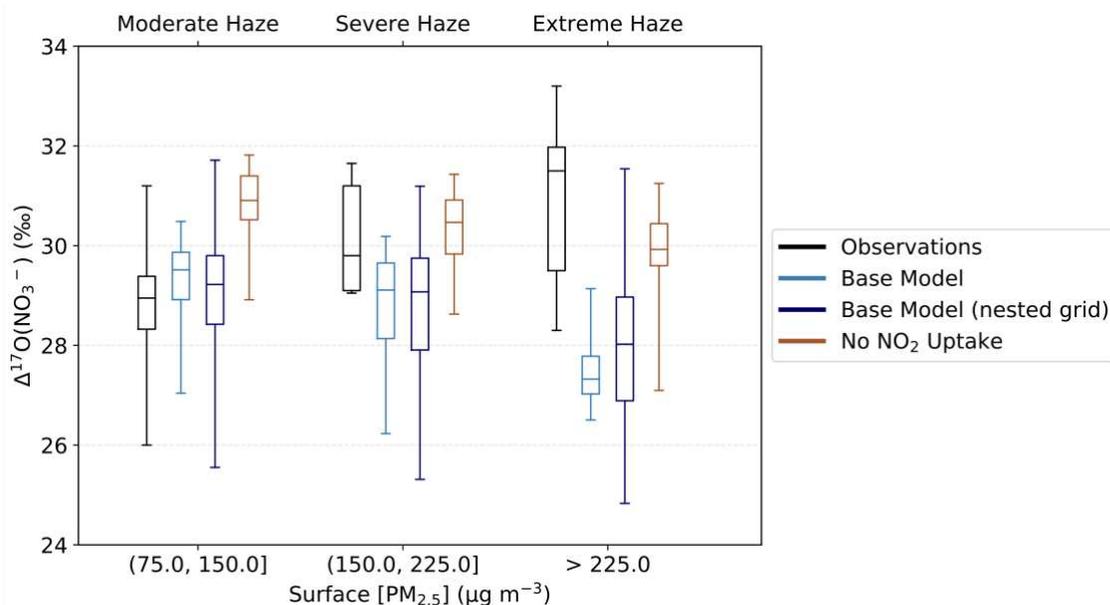
Figure 3. Comparison of $\Delta^{17}O(NO_3^-)$ in observations and model simulations under different haze regimes.

424

Figure 4. Concentration and speciation of O_x under different haze regimes in (a) observations, (b) base simulation, (c) nested-grid base simulation, (d) No NO_2 Uptake simulation. Hatching (x-filled bars) indicates the O_x species that were not measured at the observation sites.

425
426

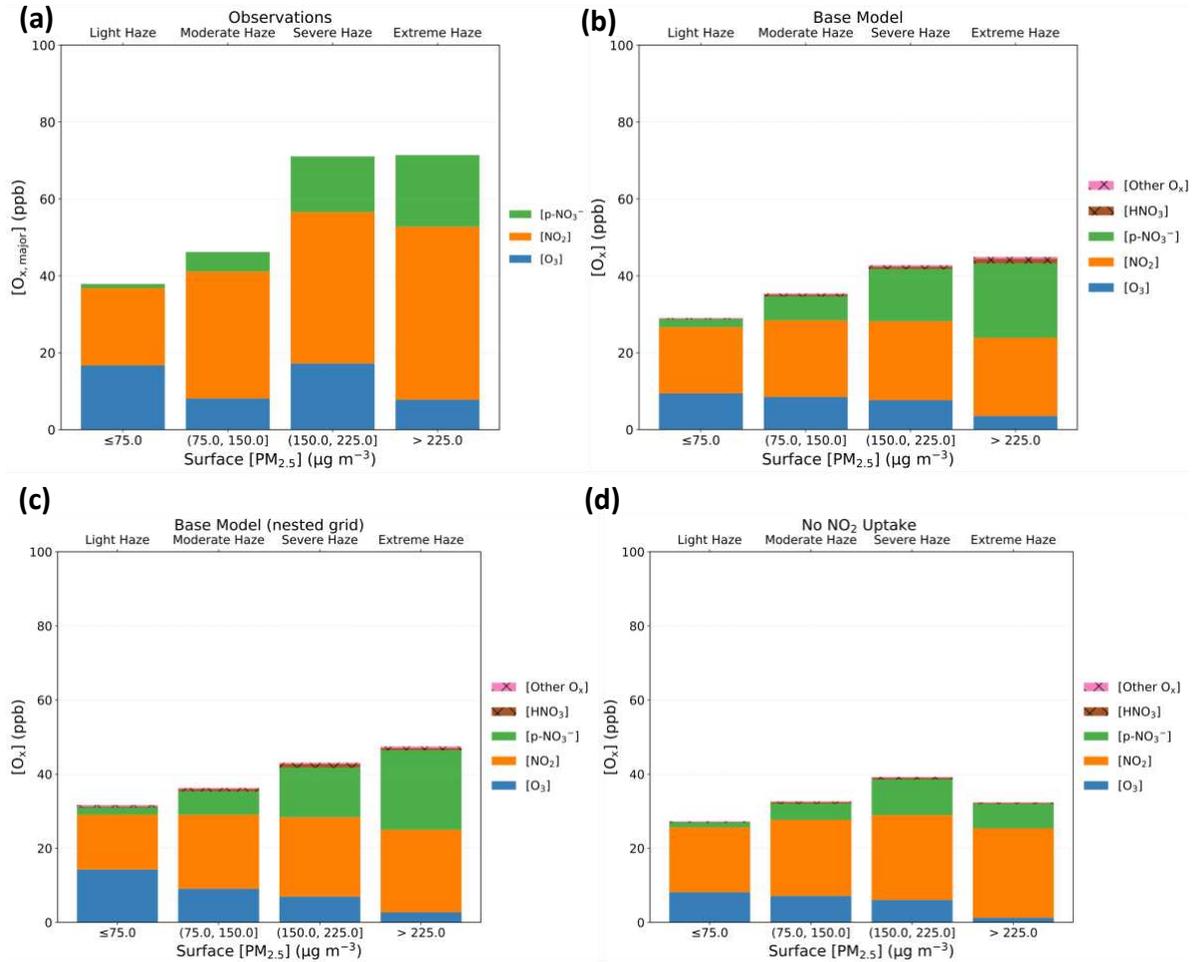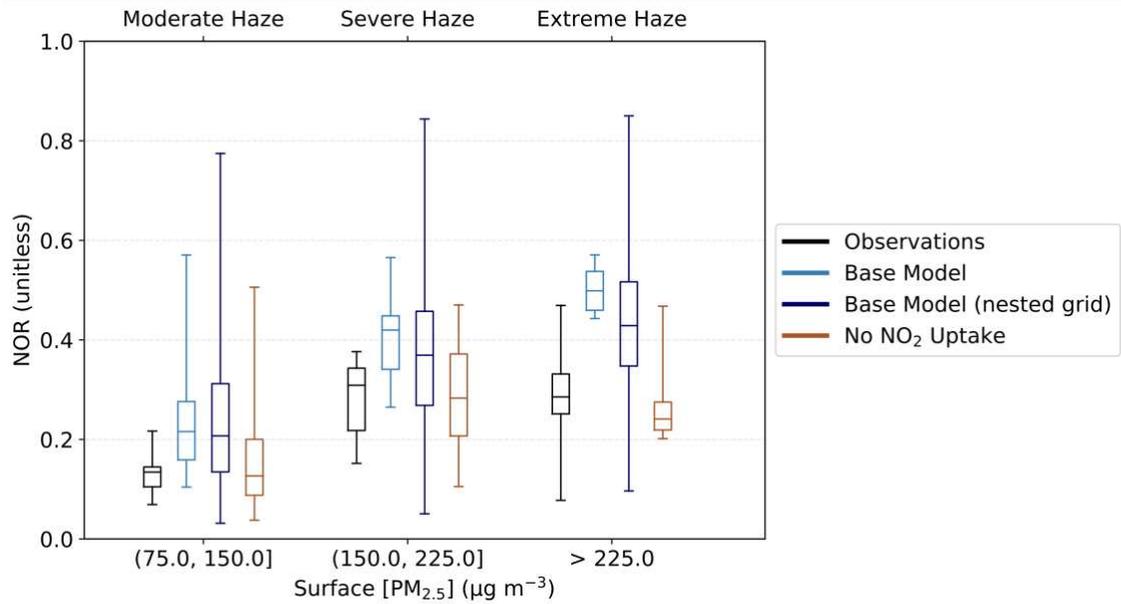**Figure 5.** Comparison of nitrogen oxidation ratio (NOR) in observations and model simulations under different haze regimes.
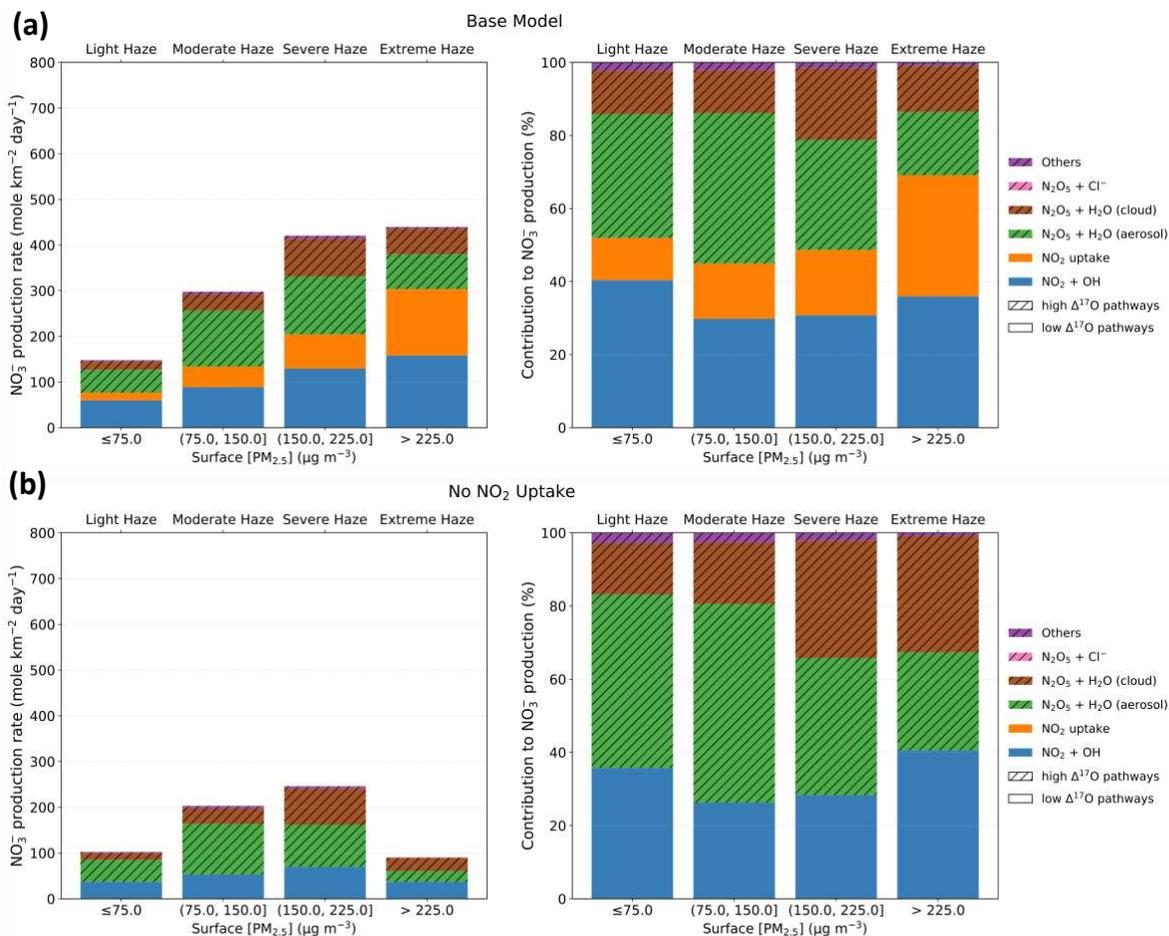
427

Figure 6. Average rate of different near-surface nitrate production pathways (left) and their relative contribution to nitrate formation in Beijing under different haze regimes (right) in (a) the base simulation and (b) No NO_2 Uptake simulation. "Near-surface" is defined as the sum over the ten lowest vertical levels in model, which on average corresponds to the altitudes between 0 to 1300 m. Hatching (//-filled bars) indicates high-$\Delta^{17}O$ pathways.

428

429

3.2.2 No-NO₂-uptake model simulation

431

An overestimate of NOR combined with the models' low bias in $\Delta^{17}O$ suggests an overestimate of NO_2 uptake (a low-$\Delta^{17}O$ heterogeneous pathway). Although a high bias in NOR could also suggest an underestimate of renoxification, a model sensitivity study allowing for efficient photolysis of p-NO_3^- shows that this explanation cannot resolve the model biases (Refer to Text S2.1 in SI). To evaluate the role of NO_2 uptake on the three chemistry metrics, we perform a sensitivity simulation in which the reaction is removed from the model by setting the uptake coefficients of NO_2 uptake on all types of aerosol and clouds to zero (i.e., $\gamma(NO_2) = 0$).

439

Without NO_2 uptake, the model predicts higher $\Delta^{17}O(NO_3^-)$ relative to the base model simulation under all haze regimes (Figure 3). The average increase in modeled $\Delta^{17}O(NO_3^-)$ in intense haze is 1.5 ‰, and the largest increase is found in extreme haze: the modeled median $\Delta^{17}O(NO_3^-)$ increases by 2.6 ‰ compared to the base simulation. Most of the modeled $\Delta^{17}O(NO_3^-)$ in

444   extreme haze now lie inside the range of observations. The simulation without NO_2 uptake
445   predicts the median $\Delta^{17}O(NO_3^-)$ in extreme haze to be 29.9‰, which is closer to the
446   observations (31.5‰). However, the model now overestimates the $\Delta^{17}O(NO_3^-)$ in moderate haze.
447   The median $\Delta^{17}O(NO_3^-)$ in moderate haze in the model is 30.9‰, which is 2.0‰ higher than the
448   observations. Similar to the base simulation, the simulation without NO_2 uptake predicts a
449   decrease in $\Delta^{17}O(NO_3^-)$ as $[PM_{2.5}]$ increases. The negative relationship is driven by the sharp
450   decrease in the rate of N_2O_5 production and nitrate production via N_2O_5 uptake in extreme haze
451   (Figure 6).
452
453   The model without NO_2 uptake shows better agreement with observations of O_x speciation and
454   NOR but still underestimates the total O_x concentration (Figure 4 and Figure 5). The average
455   NOR in intense haze in the model is 0.22, which is very close to the observations (0.21). The
456   modeled NOR in extreme haze spans within the observed range for all haze regimes (Figure 5).
457   Modeled $[O_x]$ is not sensitive to the change in NO_2 uptake, except in extreme haze. $[O_x]$ in
458   extreme haze decreases from 41.0 ppb in the base simulation to 34.6 ppb in the simulation with
459   no NO_2 uptake. This worsens the underestimate of modeled $[O_x]$.
460
461   The reduction in NOR relative to the base model simulation is due to a reduction in the nitrate-
462   production rate in all haze regimes, but especially during extreme haze (Figure 6). This is driven
463   mainly by the absence of NO_2 uptake as a nitrate-production pathway, but also due to a decrease
464   in nitrate production via $NO_2 + OH$. The decrease in nitrate production via $NO_2 + OH$ is driven
465   by the lack of HONO production from NO_2 uptake, the photolysis of which was a major source
466   of OH in the model. The rate of N_2O_5 uptake remains relatively unchanged, except for a decrease
467   during extreme haze (Figure 7). This increases the relative importance of N_2O_5 uptake resulting
468   in an increase in $\Delta^{17}O(NO_3^-)$ during all haze regimes compared to the base model, especially
469   during more intense haze events.
470
471   The results from the simulation without NO_2 uptake demonstrates that model discrepancies in
472    $\Delta^{17}O(NO_3^-)$ and O_x as seen in the base simulation cannot be solely explained by the uncertainty
473   in the efficiency of NO_2 uptake. Even when we completely eliminate the contribution of nitrate
474   production from the NO_2 uptake pathway, the existing high-$\Delta^{17}O$ pathways in the model still
475   cannot contribute enough to reproduce the observed range of $\Delta^{17}O(NO_3^-)$ in severe haze and
476   extreme haze. This model sensitivity simulation also shows that the supply of $[NO_2]$ is not a rate-
477   limiting factor for N_2O_5 uptake in Beijing. As less NO_2 is converted into NO_3^- due to the absence
478   of NO_2 uptake pathway, the modeled $[O_3]$ becomes more depleted as $[NO_x]$ increases (Figure 4
479   and Figure S6). In the presence of excess NO_x, the low $[O_3]$ in the model slows down the
480   production of NO_3 radicals via $NO_2 + O_3$, which ultimately limits the rate of N_2O_5 production via
481    $NO_2 + NO_3$ and nitrate production via N_2O_5 uptake. Compared with the base simulation, the
482   simulation without NO_2 uptake predicts lower N_2O_5 production and lower nitrate production via
483   N_2O_5 uptake on aerosols and clouds in extreme haze (Figure 7), further supporting that O_3 is the
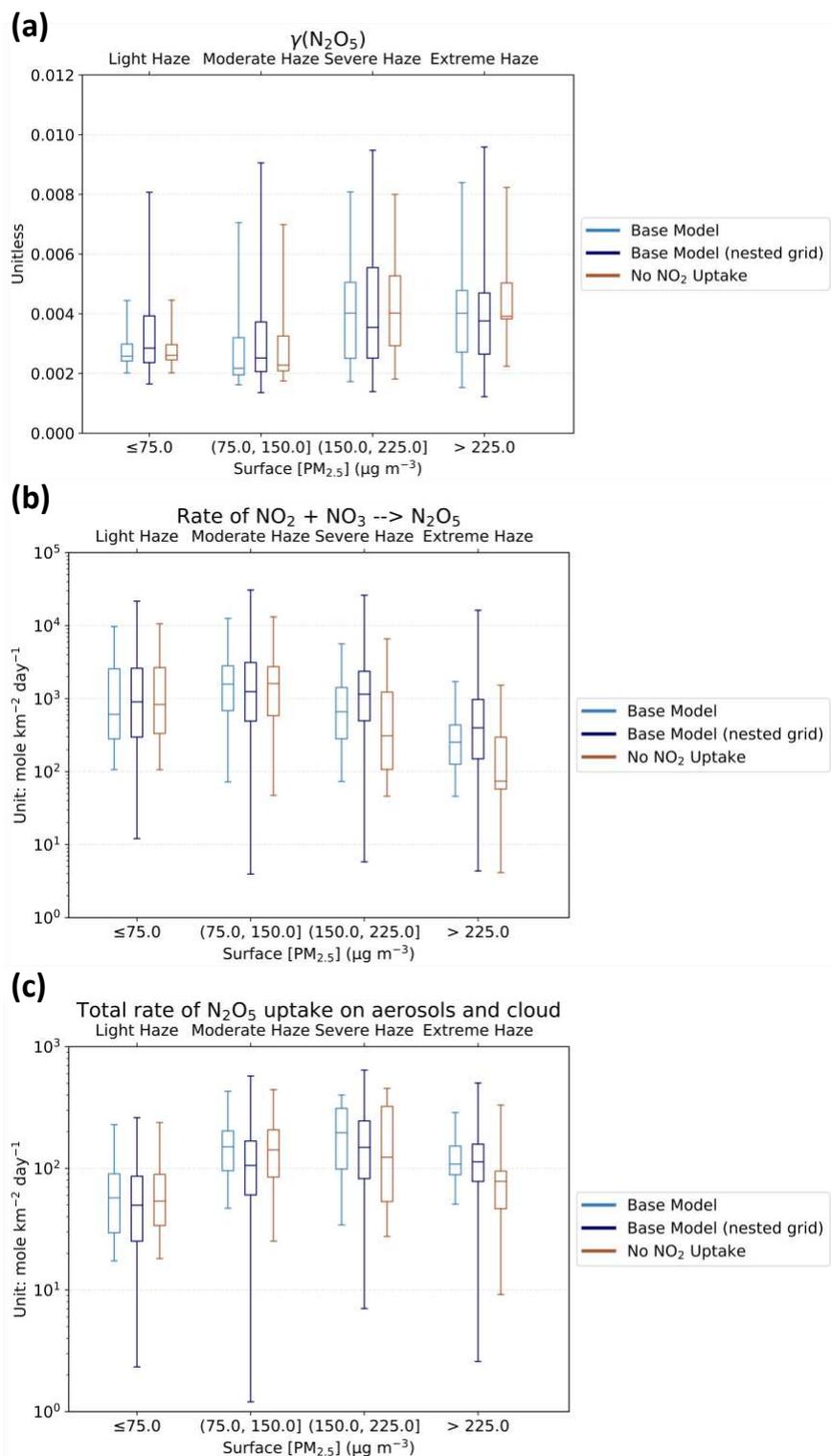484   limiting factor for N_2O_5 production and uptake.
485
486

Figure 7. Factors controlling the near-surface rate of nitrate production via N_2O_5 hydrolysis in simulations and their dependence on [$PM_{2.5}$]. 7(a) shows the average uptake coefficient of N_2O_5 on aerosols. 7(b) shows the average rate of N_2O_5 production. 7(c) shows the average total rate of N_2O_5 uptake on aerosols and cloud.

488   **4 Discussion**

489

490   **4.1 Model sensitivity to uncertainties in NO_2 uptake on aerosol**

491

492   The model results presented in Section 3 and Text S2 show that modeled NOR and $\Delta^{17}O(NO_3^-)$
493   are most sensitive to NO_2 uptake. In NO_x-rich air, we expect to see positive relationships
494   between $[HO_x]$ and $[O_3]$ because of their coupling via the cycling of NO_x (Bates & Jacob, 2020).
495   As modeled O_3 concentration increases, NO more likely reacts with O_3 to produce NO_2, as a
496   result, more HO_x becomes available for other reactions, including nitrate production, and vice
497   versa. The competing effects of HO_x- and ozone-related nitrate-production pathways explain
498   why modeled $\Delta^{17}O(NO_3^-)$ is not very sensitive to changes in various chemical parameters, with
499   the exception of $\gamma(NO_2)$. NO_2 uptake, which carries a low-$\Delta^{17}O$ signature, is the only important
500   nitrate-production pathway in the base model that converts NO_2 into NO_3^- without involving
501   HO_x or ozone directly (Figure 1b). Additional model simulations increasing the HONO yield
502   resulting from NO_2 uptake on aerosol to 100%, as well as model simulations including various
503   combinations of the three model sensitivity studies described in Section 3.2 and Text S2, further
504   show that $\Delta^{17}O(NO_3^-)$ and NOR are most sensitive to $\gamma(NO_2)$ (Figure S9 and Figure S10). The
505   extra HONO produced from NO_2-uptake yielding 100% HONO increases OH and the rate of
506    $NO_2 + OH$ and simultaneously promotes nitrate production via N_2O_5 uptake through HO_x-O_3
507   coupling effects (See Figure S11), but the modeled $[O_x]$ is still low compared to the observations
508   (Figure S12). Among all the model simulations performed, only those with $\gamma(NO_2) = 0$ improve
509   model agreement with both observed $\Delta^{17}O(NO_3^-)$ and NOR during more intense haze events
510   (Figure S9 and Figure S10).

511

512   In addition to the isotopic constraints, results from some laboratory and field studies also support
513   the choice of a lower $\gamma(NO_2)$. The current GC parametrization sets $\gamma(NO_2, black carbon)=10^{-4}$,
514   which is 20 times higher than $\gamma(NO_2, SNA)$. Laboratory studies of $NO_2(g)$ uptake on soot or
515   carbonaceous surfaces suggested that heterogeneous reactions can rapidly consume the organic
516   adsorbates and/or surface groups (Ammann et al., 1998; Bröske et al., 2003; Gerecke et al.,
517   1998; Kalberer et al., 1999; Kleffmann et al., 1999), with rates of NO_2 uptake decreasing to
518   negligible levels within minutes to hours (Gerecke et al., 1998; Kalberer et al., 1999; Kleffmann
519   et al., 1999). For SNA aerosols, laboratory studies by F. Tan et al. (2016) and F. Tan et al. (2017)
520   found that the rate of NO_2 uptake decreases with increasing RH when aerosols contain $CaCO_3$
521   due to formation of insoluble $CaSO_4 \cdot nH_2O$ on aerosol surfaces at higher RH. A potential
522   suppressing effect of high-RH conditions on NO_2 uptake may help to explain the positive
523   relationship between $\Delta^{17}O(NO_3^-)$ and $[PM_{2.5}]$ in observations. P. Liu et al. (2020) used the RH-
524   dependence of NO_2 uptake to explain the negative relationship between NOR and RH when RH
525   is above 60% in their Beijing observations. However, we cannot replicate their finding using our
526   observations, which show a positive relationship between NOR and RH across all RH conditions
527   (Figure S13). While some studies suggested that the heterogeneous reactions between NO_2 and
528   SO_2 are important during wintertime haze events (e.g., Cheng et al., 2016; J. Wang et al., 2020),
529   analysis of sulfate $\Delta^{17}O$ observations by Shao et al. (2019) showed that these reactions contribute
530   less than 2% to heterogeneous formation of sulfate based on isotope observations in Beijing
531   during the time period studied here. Given the large uncertainties of NO_2 uptake under
532   atmospheric conditions and its large influence on nitrate production, HONO production, and $[O_x]$

533 in extreme haze, future studies should investigate the dominant mechanisms of NO_2 uptake on
534 ambient aerosols and seek additional observational constraints during more intense haze events.
535
536

537 **4.2 Possible causes of modeled underestimate in wintertime $[O_x]$ in the North China Plain**
538 **and their potential influence on NO_y chemistry**
539

540 The model bias in wintertime ozone is critical for the simulation of $[O_x]$ and nitrate production
541 via N_2O_5 uptake. NO_2 and ozone are the major components of $[O_x]$, but the base model
542 underestimates their concentration in Beijing, especially during intense haze events. Modeled
543 $[NO_x]$ increases with $[PM_{2.5}]$ in Beijing, and NO becomes the primary NO_x species in severe and
544 extreme haze (Average $[NO]/[NO_x]$ ratios are 0.55 and 0.66, respectively, in the base model. See
545 Figure S6). The high $[NO]/[NO_x]$ ratio on more polluted days is also evident in other wintertime
546 observations in Beijing (Lu et al., 2019; Jiaqi Wang et al., 2017; G. Zhang et al., 2020). Under
547 NO_x-saturated regime, the daytime cycling of NO and NO_2 is mainly controlled by the rates of
548 $NO + O_3$ reaction (R3, a.k.a. ozone titration) and NO_2 photolysis. As predicted by the Leighton
549 Relationship, $[NO_2]/[NO]$ ratio is linearly proportional to $[O_3]$ at photochemical steady state.
550 From this basic theoretical perspective, the model bias in wintertime ozone should at least partly
551 explain the underestimate in $[NO_2]$ in our simulations. The actual NO_x-O_3 relationship may
552 deviate from Leighton's prediction because of the complicated interaction between aerosols and
553 radiation, which can affect the photolysis of NO_2 and O_3 (Hollaway et al., 2019; W. Wang et al.,
554 2019). As explained in Section 3.2, low $[O_3]$ can also limit nitrate production via N_2O_5 uptake in
555 NO_x-rich air. Since ozone is a secondary pollutant that plays a central role in tropospheric
556 chemistry, the formation of ozone is inevitably sensitive to many different chemical processes.
557 The particulate-nitrate-photolysis and chlorine-chemistry simulations show improvement in
558 reproducing $[O_3]$ in intense haze in Beijing compared to the base simulation, but none of the
559 proposed updates to NO_y and Cl_y chemistry investigated here can completely correct the model's
560 overall bias in O_x in Beijing (See Figure S12 and Text S2). In this section, we discuss other
561 chemical processes that may explain the modeled underestimate in wintertime $[O_3]$ and $[O_x]$.
562
563

564 **4.2.1 Aerosol uptake of HO_2 radicals**
565

566 The uptake of HO_2 radicals on aerosols has been suggested as a key process in driving the
567 observed trends of ozone in China in the 2010s (J. Li et al., 2018; K. Li, Jacob, Liao, Shen, et al.,
568 2019; K. Li, Jacob, Liao, Zhu, et al., 2019). Aerosols can scavenge gas-phase HO_2 radicals
569 reducing $[HO_x]$ and inhibiting ozone production. As pollution-control policies in China have
570 reduced ambient $[PM_{2.5}]$ in the 2010s, less HO_2 is scavenged by aerosols, resulting in increases
571 in the ozone production efficiency. This theory on HO_x-O_3-aerosol interactions is consistent with
572 the increasing trend of summertime ozone observed in China (K. Li, Jacob, Liao, Shen, et al.,
573 2019; K. Li, Jacob, Liao, Zhu, et al., 2019).
574

575 Despite the potential impacts of aerosol uptake of HO_2 on ozone in urban air, the efficiency of
576 this chemical process is still highly uncertain and may strongly depend on the content of aqueous
577 transition-metal ions, the acidity, and the size of the aerosol (Guo et al., 2019; Mao et al., 2013;
578 Thornton & Abbatt, 2005). To estimate the largest possible influence of HO_2 uptake on model

579   bias in $[O_x]$ in intense haze, we consider the extreme case of $\gamma(HO_2) = 0$ on all aerosols (Denote
580   as no HO_2 uptake simulation). Disabling the uptake of HO_2 on aerosols increases the modeled
581   median $[O_{x,\,major}]$ by 9.5% in intense haze, but this is smaller than the corresponding change
582   resulting from introducing p-NO_3^- photolysis into the model (+24%) (See Figure S12 and Text
583   S2). The model still fails to reproduce the high level of $[O_x]$ in observations in intense haze. The
584   overall effect of HO_2 uptake on NOR and $\Delta^{17}O(NO_3^-)$ are small in comparison with the models
585   with $\gamma(NO_2) = 0$ (See Figure S9 and Figure S10). Our simulation results show that the
586   uncertainty in $\gamma(HO_2)$ is not of primary importance to the model bias in simulating $[O_x]$, NOR,
587   and $\Delta^{17}O(NO_3^-)$ in Beijing.
588
589
590   **4.2.2 Wintertime emissions of volatile organic compounds in the North China Plain**
591
592   The roles of VOCs in nitrate production have been highlighted in recent studies of nitrate
593   pollution in urban air (Fu et al., 2020; He et al., 2018; Shah et al., 2020; W. Song et al., 2020; Y.
594   Wang et al., 2019; Womack et al., 2019). In Text S1, we showed that the direct effects of VOCs
595   on nitrate formation are likely small in wintertime Beijing. However, VOCs can still modulate
596   nitrate production rates by influencing ozone formation (Huang et al., 2021; Womack et al.,
597   2019). VOCs accelerate the production of O_3 in NO_x-rich urban air. Reduction in VOC emissions
598   has been proposed as a key strategy for mitigating wintertime nitrate pollution in Beijing and in
599   Utah (Lu et al., 2019; Womack et al., 2019). Because of the potential importance of [VOCs] in
600   nitrate production during intense haze events, we investigate the model bias in simulating
601   wintertime [VOCs] in Beijing and examine whether a bias in [VOCs] can explain the model-
602   observation discrepancy in terms of $[O_x]$.
603
604   Emitted from biomass burning and fossil fuels, aromatic compounds are often considered to be
605   the largest contributor to ozone formation in metropolitan areas in China (J. Sun et al., 2018; Yan
606   et al., 2017; D. Yu et al., 2020). The concentration of aromatics in general positively correlates
607   with $[PM_{2.5}]$ in the model (Table S3), consistent with observations in the North China Plain (C.
608   Liu et al., 2017; Sheng et al., 2018; J. Sun et al., 2018). However, the model underestimates the
609   concentration of aromatics compared to the observations, except for xylene. The mean
610   concentration of benzene in the base simulation is lower than the wintertime observations in
611   Beijing by a factor of 2 (see Table S3). Le et al. (2020) showed that a 30% increase in the
612   emissions of VOCs from conventional anthropogenic sources can increase the wintertime $[O_3]$
613   by about 10% in their model. Model bias in wintertime VOC emissions from industry and
614   transportation could be an important reason for the underestimate of modeled $[O_x]$ during intense
615   haze events.
616
617   Recent studies suggested that the manufacture and consumption of volatile chemical products
618   (VCPs) can be an overlooked anthropogenic VOC-emission source in air-quality models (e.g.,
619   McDonald et al., 2018). Throughout the product life cycle, these VCPs emit many complex
620   VOCs, including C$\geq$4 alkanes, alcohols, and terpenes, and may account for about half of the
621   VOC reactivity with OH in Los Angeles (McDonald et al., 2018). Comparison of the
622   concentration of these VCP-related VOCs in the base simulation with wintertime observations in
623   Beijing shows a model underestimate of the concentration of alcohols, monoterpenes, and C$\geq$4
624   alkanes in Beijing (See Table S3). However, without more observational constraints on the fluxes

625 and speciation of VCP emissions in the North China Plain and their dependencies on atmospheric
626 conditions, it is hard to conclude whether the model bias in [O_x] can be reduced by including
627 emissions of VCPs in the simulations.
628
629
630 **4.3 Examination of the non-linearity in nitrate chemistry**
631
632 The weak response of particulate nitrate and other secondary aerosols to the reduction in NO_x
633 emissions has been noted in studies of the long-term trends in wintertime air quality (e.g., H. Li
634 et al., 2019; Shah et al., 2018; Xu et al., 2019), and more recently, in studies of air quality during
635 the COVID-19 pandemic (Diamond & Wood, 2020; Huang et al., 2021; Le et al., 2020; Y. Sun
636 et al., 2020). An astonishing example of the complexity of this NO_x-aerosol relationship can be
637 found in the observations in the North China Plain from January to March in year 2020.
638 Following a 40-60% reduction in the NO_x emissions over the North China Plain caused by
639 COVID-19 lockdown, observed [$PM_{2.5}$], paradoxically, increased by 50% or more at several
640 stations near Beijing (Huang et al., 2021; Le et al., 2020). Studies suggested that the surge is
641 mostly driven by the production of secondary aerosols, including p-NO_3^- (Huang et al., 2021; Le
642 et al., 2020).
643
644 Many studies attributed the persistence of high levels of p-NO_3^- to the non-linearity in
645 atmospheric chemistry, but they hypothesized different mechanisms. Shah et al. (2018)
646 suggested that NO_x and SO_2 emission reductions over the eastern United States has resulted in a
647 gradual increase in aerosol alkalinity, which favors HNO_3-to-p-NO_3^- conversion and increases
648 the fraction of p-NO_3^- in wintertime aerosols. We denote the non-linearity originated from the
649 sensitivity of p-NO_3^- to aerosol-pH as the 'alkalinity-limited mechanism'. In contrast, studies in
650 China observed an increase in [O_3] and production of secondary aerosols following the emission
651 reductions during COVID-19 lockdown, which is likely caused by a reduction in ozone titration
652 (Huang et al., 2021; Le et al., 2020). The enhancement in [O_3] increases the oxidizing capacity of
653 the lower troposphere and promotes the production of secondary aerosols (Fu et al., 2020; Huang
654 et al., 2021; Le et al., 2020). We denote the non-linearity arising from the sensitivity of nitrate to
655 NO_x-VOCs-ozone chemistry as the 'ozone-limited mechanism'.
656
657 To examine the relevance of ozone-limited mechanism in our model simulations of nitrate
658 production, we analyze the relationship between nitrate production rate, [O_3], and [NO_x] during
659 intense haze events for Beijing (Figure 8). It is noted that the inter-model differences in our study
660 orginates from the variations in the modeled chemistry. This is different from other studies like
661 Huang et al. (2021), where they focused on the effects of changing emissions. Although the
662 modeled [O_3], [NO_x], and nitrate production rate are considerably different among various
663 experiments, a positive relationship between nitrate production rate and [O_3] during intense haze
664 events can be identified in all the simulations with $\gamma(NO_2) = 0$. In contrast, all these simulations
665 predict a negative relationship between the nitrate production rate and [NO_x], which can be
666 attributed to the effects of ozone titration. The strong and postive correlation between the nitrate
667 production rate and [O_3] predicted by our models is consistent with the theory of ozone-limited
668 mechanism. Meanwhile, our simulations also show that the partitioning between p-NO_3^- and
669 HNO_3 in Beijing is not sensitive to the intensity of haze events or the difference in NO_y
670 chemistry parametrization (See Figure S14). p-NO_3^- remains the dominant form of NO_3^- in all

671 cases. The model prediction is also consistent with the estimated high aerosol pH (4.5 ± 0.7) in
672 wintertime Beijing, which can be explained by the high NH_3 abundance in observations (Ding et
673 al., 2019). Our model simulations confirm the importance of ozone-limited mechanism in
674 wintertime North China Plain and show that the positive relationship between $[O_3]$ and nitrate
675 production rate during intense haze events is robust regardless of the uncertainty in modeled NO_y
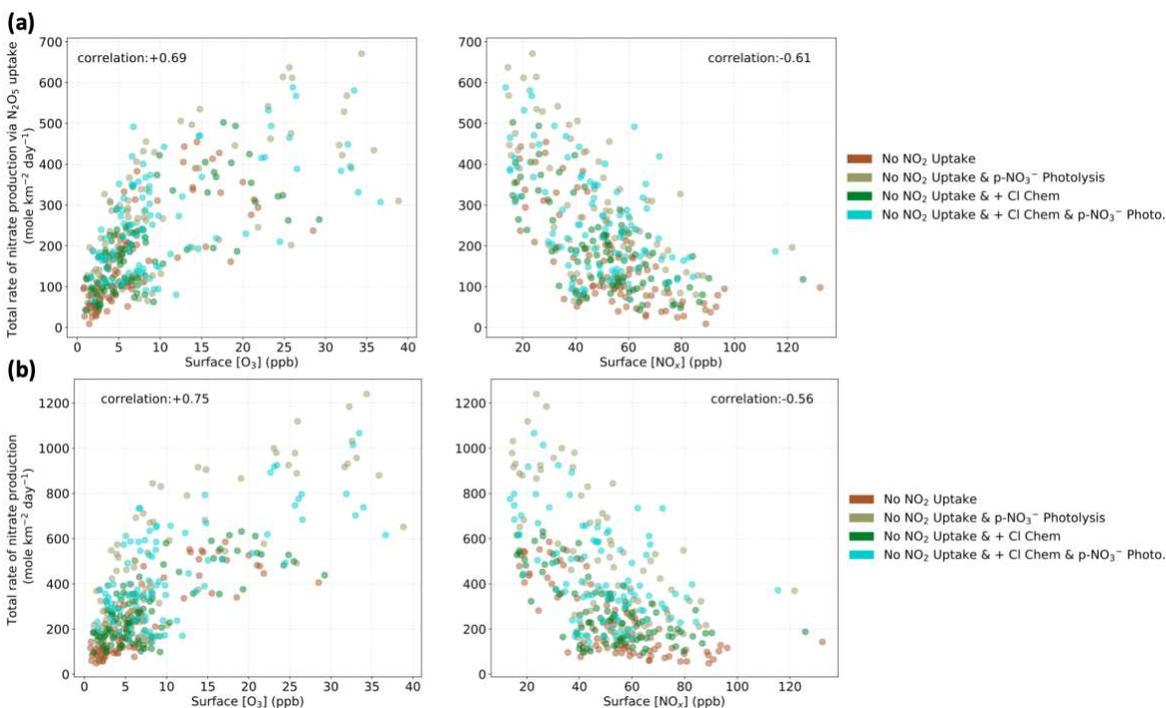676 chemistry after $\gamma(NO_2)$ is set to 0.

677

Figure 8. The relationship between $[O_3]$, $[NO_x]$, the rate of nitrate production via N_2O_5
uptake (8a), and the total rate of nitrate production (8b) during intense haze events in
simulations without NO_2 uptake on aerosols. The correlation coefficients shown in the
figure are calculated using data from all the four model experiments. All the estimated
linear-regression slopes are different from 0 at the 95% significance level.

678
679

5 Conclusions and Implications

681

682 By analyzing the observations of $\Delta^{17}O(NO_3^-)$, NOR, and O_x in Beijing during winter 2014-15
683 and results from a global and regional chemical transport model, we examine the mechanisms for
684 nitrate production in wintertime North China Plain and how the underlying chemical processes
685 vary with the intensity of haze events. $\Delta^{17}O(NO_3^-)$ indicates the dominance of high-$\Delta^{17}O$
686 oxidants (e.g., ozone) to low-$\Delta^{17}O$ oxidants (e.g., OH and RO_2) during NO_x-to-NO_3^- conversion,
687 while NOR and O_x provide information about the efficiency of NO_y oxidation and the oxidizing
688 capacity of the air. In intense haze, the base model underestimates $\Delta^{17}O(NO_3^-)$ and $[O_x]$ in
689 Beijing by -0.86 ‰ and -36%, respectively, but overestimates NOR by $+0.12$. To investigate
690 the relationship between model bias and uncertainty in chemistry, we perform model sensitivity
691 experiments by varying several key parameters in NO_y chemistry. Our analysis suggests a model

692 overestimate in NO$_2$-uptake rate on aerosols and the underestimate in wintertime ozone may
693 explain the model biases.
694
695 Our model sensitivity simulations show that modeled $\Delta^{17}O(NO_3^-)$ and NOR during highly
696 polluted conditions are most sensitive to the parametrization of NO$_2$ uptake on aerosols. The
697 $\Delta^{17}O(NO_3^-)$ observations in Beijing and its relationship with [PM$_{2.5}$] suggest that the rate of NO$_2$
698 uptake is likely too high in the model, yielding too high nitrate- and HONO-production rates in
699 more intense haze. Model simulations without NO$_2$ uptake better reproduce the observed
700 $\Delta^{17}O(NO_3^-)$ and NOR in Beijing under high-PM$_{2.5}$ conditions. A NO$_2$ uptake mechanism that is
701 suppressed by high RH may explain the positive relationship between $\Delta^{17}O(NO_3^-)$ and [PM$_{2.5}$] in
702 observations, but the supporting evidence for such a mechanism is currently inconclusive.
703 Further laboratory and field studies are needed to constrain the reaction probability of NO$_2$ on
704 ambient aerosols, with a focus on its role in nitrate and HONO formation.
705
706 Our simulations also reveal that nitrate production is largely limited by ozone during intense
707 haze events in wintertime North China Plain. After accounting for the uncertainty in NO$_2$ uptake
708 on aerosols, our analysis suggests that N$_2$O$_5$ uptake in aerosols and clouds is the dominant
709 mechanism for nitrate production in wintertime Beijing. Under high-NO$_x$-high-PM$_{2.5}$ conditions,
710 [O$_3$] modulates N$_2$O$_5$ production and, subsequently, the rate of nitrate production via N$_2$O$_5$
711 uptake. The base model underestimates [O$_3$] and [O$_x$] during wintertime haze events. Uncertainty
712 in heterogeneous chemical processes, such as renoxification via nitrate photolysis or ClNO$_2$
713 production and the scavenging of HO$_x$ by aerosols, may contribute to the model bias in
714 wintertime O$_x$, but our simulations show that adjusting related chemistry parameters cannot
715 remove the bias even under extreme scenarios, suggesting processes other than chemistry (e.g.,
716 emissions of VCPs and feedbacks involving aerosol-boundary-layer interaction) may play a
717 more important role. Both the reduction in [PM$_{2.5}$] and NO$_x$ emissions have been shown to lead
718 to increases in [O$_3$] in the North China Plain (Huang et al., 2021; Le et al., 2020; K. Li, Jacob,
719 Liao, Zhu, et al., 2019). Nitrate production rates may continue to increase as long as [O$_3$]
720 increases despite decreases in [NO$_x$], creating a negative feedback that reduces the effectiveness
721 of air pollution reduction strategies. Policies that result in a reduction of ambient O$_3$
722 concentrations, possibly through reductions in VOC emissions, will also reduce the formation of
723 nitrate and its contribution to PM$_{2.5}$ during wintertime haze events.
724
725

737   University of Washington's ResearchWorks Archive and can be accessed online

738   (http://hdl.handle.net/1773/46927).

739

References

740 **References**

741 Alexander, B., Sherwen, T., Holmes, C. D., Fisher, J. A., Chen, Q., Evans, M. J., & Kasibhatla,
742 P. (2020). Global inorganic nitrate production mechanisms: comparison of a global model
743 with nitrate isotope observations. *Atmospheric Chemistry and Physics*, *20*(6), 3859–3877.
744 https://doi.org/10.5194/acp-20-3859-2020

745 Ammann, M., Kalberer, M., Jost, D. T., Tobler, L., Rössler, E., Piguet, D., et al. (1998).
746 Heterogeneous production of nitrous acid on soot in polluted air masses. *Nature*, *395*(6698),
747 157–160. https://doi.org/10.1038/25965

748 An, Z., Huang, R.-J., Zhang, R., Tie, X., Li, G., Cao, J., et al. (2019). Severe haze in northern
749 China: A synergy of anthropogenic emissions and atmospheric processes. *Proceedings of*
750 *the National Academy of Sciences of the United States of America*, *116*(18), 8657–8666.
751 https://doi.org/10.1073/pnas.1900125116

752 Bao, F., Li, M., Zhang, Y., Chen, C., & Zhao, J. (2018). Photochemical Aging of Beijing Urban
753 PM $_{2.5}$: HONO Production. *Environmental Science & Technology*, *52*(11), 6309–6316.
754 https://doi.org/10.1021/acs.est.8b00538

755 Bates, K. H., & Jacob, D. J. (2020). An Expanded Definition of the Odd Oxygen Family for
756 Tropospheric Ozone Budgets: Implications for Ozone Lifetime and Stratospheric Influence.
757 *Geophysical Research Letters*, *47*(4). https://doi.org/10.1029/2019GL084486

758 Bertram, T. H., & Thornton, J. A. (2009). Toward a general parameterization of N2O5 reactivity
759 on aqueous particles: The competing effects of particle liquid water, nitrate and chloride.
760 *Atmospheric Chemistry and Physics*, *9*(21), 8351–8363. https://doi.org/10.5194/acp-9-8351-
761 2009

762 Bröske, R., Kleffmann, J., & Wiesen, P. (2003). Heterogeneous conversion of NO2 on secondary
763 organic aerosol surfaces: A possible source of nitrous acid (HONO) in the atmosphere?
764 *Atmospheric Chemistry and Physics*, *3*(3), 469–474. https://doi.org/10.5194/acp-3-469-2003

765 Chen, S., Wang, H., Lu, K., Zeng, L., Hu, M., & Zhang, Y. (2020). The trend of surface ozone in
766 Beijing from 2013 to 2019: Indications of the persisting strong atmospheric oxidation
767 capacity. *Atmospheric Environment*, *242*, 117801.
768 https://doi.org/10.1016/j.atmosenv.2020.117801

769 Chen, Y., Ebenstein, A., Greenstone, M., & Li, H. (2013). Evidence on the impact of sustained
770 exposure to air pollution on life expectancy from China's Huai River policy. *Proceedings of*
771 *the National Academy of Sciences of the United States of America*, *110*(32), 12936–12941.
772 https://doi.org/10.1073/pnas.1300018110

773 Cheng, Y., Zheng, G., Wei, C., Mu, Q., Zheng, B., Wang, Z., et al. (2016). Reactive nitrogen
774 chemistry in aerosol water as a source of sulfate during haze events in China. *Science*
775 *Advances*, *2*(12), e1601530. https://doi.org/10.1126/sciadv.1601530

776 Diamond, M. S., & Wood, R. (2020). Limited Regional Aerosol and Cloud Microphysical
777 Changes Despite Unprecedented Decline in Nitrogen Oxide Pollution During the February
778 2020 COVID-19 Shutdown in China. *Geophysical Research Letters*, *47*(17).
779 https://doi.org/10.1029/2020GL088913

780 Ding, J., Zhao, P., Su, J., Dong, Q., Du, X., & Zhang, Y. (2019). Aerosol pH and its driving

781   factors in Beijing. *Atmospheric Chemistry and Physics*, *19*(12), 7939–7954.
782   https://doi.org/10.5194/acp-19-7939-2019

783 Eastham, S. D., Weisenstein, D. K., & Barrett, S. R. H. (2014). Development and evaluation of
784   the unified tropospheric–stratospheric chemistry extension (UCX) for the global chemistry-
785   transport model GEOS-Chem. *Atmospheric Environment*, *89*, 52–63.
786   https://doi.org/10.1016/j.atmosenv.2014.02.001

787 Fisher, J. A., Atlas, E. L., Barletta, B., Meinardi, S., Blake, D. R., Thompson, C. R., et al. (2018).
788   Methyl, Ethyl, and Propyl Nitrates: Global Distribution and Impacts on Reactive Nitrogen
789   in Remote Marine Environments. *Journal of Geophysical Research: Atmospheres*, *123*(21),
790   12,429-12,451. https://doi.org/10.1029/2018JD029046

791 Fountoukis, C., & Nenes, A. (2007). *Atmospheric Chemistry and Physics ISORROPIA II: a*
792   *computationally efficient thermodynamic equilibrium model for K +-Ca 2+-Mg 2+-NH +*
793   *4-Na +-SO 2− 4-NO − 3-Cl −-H 2 O aerosols*. *Atmos. Chem. Phys* (Vol. 7). Retrieved from
794   www.atmos-chem-phys.net/7/4639/2007/

795 Fu, X., Wang, T., Gao, J., Wang, P., Liu, Y., Wang, S., et al. (2020). Persistent Heavy Winter
796   Nitrate Pollution Driven by Increased Photochemical Oxidants in Northern China.
797   *Environmental Science and Technology*, *54*(7), 3881–3889.
798   https://doi.org/10.1021/acs.est.9b07248

799 Gaston, C. J., Thornton, J. A., & Ng, N. L. (2014). Reactive uptake of N_2O_5 to internally mixed
800   inorganic and organic particles: the role of organic carbon oxidation state and inferred
801   organic phase separations. *Atmospheric Chemistry and Physics*, *14*(11), 5693–5707.
802   https://doi.org/10.5194/acp-14-5693-2014

803 Geng, L., Murray, L. T., Mickley, L. J., Lin, P., Fu, Q., Schauer, A. J., & Alexander, B. (2017).
804   Isotopic evidence of multiple controls on atmospheric oxidants over climate transitions.
805   *Nature*, *546*(7656), 133–136. https://doi.org/10.1038/nature22340

806 Gerecke, A., Thielmann, A., Gutzwiller, L., & Rossi, M. J. (1998). The chemical kinetics of
807   HONO formation resulting from heterogeneous interaction of NO 2 with flame soot.
808   *Geophysical Research Letters*, *25*(13), 2453–2456. https://doi.org/10.1029/98GL01796

809 Guo, J., Wang, Z., Tao Wang, & Zhang, X. (2019). Theoretical evaluation of different factors
810   affecting the HO2 uptake coefficient driven by aqueous-phase first-order loss reaction.
811   *Science of The Total Environment*, *683*, 146–153.
812   https://doi.org/10.1016/j.scitotenv.2019.05.237

813 He, P., Xie, Z., Chi, X., Yu, X., Fan, S., Kang, H., et al. (2018). Atmospheric $\Delta^{17}O(NO_3^-)$
814   reveals nocturnal chemistry dominates nitrate production in Beijing haze. *Atmospheric*
815   *Chemistry and Physics*, *18*(19), 14465–14476. https://doi.org/10.5194/acp-18-14465-2018

816 Hoesly, R. M., Smith, S. J., Feng, L., Klimont, Z., Janssens-Maenhout, G., Pitkanen, T., et al.
817   (2018). Historical (1750–2014) anthropogenic emissions of reactive gases and aerosols
818   from the Community Emissions Data System (CEDS). *Geoscientific Model Development*,
819   *11*(1), 369–408. https://doi.org/10.5194/gmd-11-369-2018

820 Hollaway, M., Wild, O., Yang, T., Sun, Y., Xu, W., Xie, C., et al. (2019). Photochemical impacts
821   of haze pollution in an urban environment. *Atmospheric Chemistry and Physics*, *19*(15),
822   9699–9714. https://doi.org/10.5194/acp-19-9699-2019

823 Holmes, C. D., Bertram, T. H., Confer, K. L., Graham, K. A., Ronan, A. C., Wirks, C. K., &
824   Shah, V. (2019). The Role of Clouds in the Tropospheric NOx Cycle: A New Modeling
825   Approach for Cloud Chemistry and Its Global Implications. *Geophysical Research Letters*,
826   *46*(9), 4980–4990. https://doi.org/10.1029/2019GL081990

827 Huang, X., Ding, A., Wang, Z., Ding, K., Gao, J., Chai, F., & Fu, C. (2020). Amplified
828   transboundary transport of haze by aerosol–boundary layer interaction in China. *Nature
829   Geoscience*, *13*(6), 428–434. https://doi.org/10.1038/s41561-020-0583-4

830 Huang, X., Ding, A., Gao, J., Zheng, B., Zhou, D., Qi, X., et al. (2021). Enhanced secondary
831   pollution offset reduction of primary emissions during COVID-19 lockdown in China.
832   *National Science Review*, *8*(2). https://doi.org/10.1093/nsr/nwaa137

833 Hudman, R. C., Moore, N. E., Mebust, A. K., Martin, R. V, Russell, A. R., Valin, L. C., &
834   Cohen, R. C. (2012). Steps towards a mechanistic model of global soil nitric oxide
835   emissions: implementation and space based-constraints. *Atmospheric Chemistry and
836   Physics*, *12*(16), 7779–7795. https://doi.org/10.5194/acp-12-7779-2012

837 Itahashi, S., Yumimoto, K., Uno, I., Hayami, H., Fujita, S., Pan, Y., & Wang, Y. (2018). A 15-
838   year record (2001–2015) of the ratio of nitrate to non-sea-salt sulfate in precipitation over
839   East Asia. *Atmospheric Chemistry and Physics*, *18*(4), 2835–2852.
840   https://doi.org/10.5194/acp-18-2835-2018

841 Jaeglé, L., Shah, V., Thornton, J. A., Lopez-Hilfiker, F. D., Lee, B. H., McDuffie, E. E., et al.
842   (2018). Nitrogen Oxides Emissions, Chemistry, Deposition, and Export Over the Northeast
843   United States During the WINTER Aircraft Campaign. *Journal of Geophysical Research:
844   Atmospheres*, *123*(21), 12,368-12,393. https://doi.org/10.1029/2018JD029133

845 Kalberer, M., Ammann, M., Arens, F., Gäggeler, H. W., & Baltensperger, U. (1999).
846   Heterogeneous formation of nitrous acid (HONO) on soot aerosol particles. *Journal of
847   Geophysical Research: Atmospheres*, *104*(D11), 13825–13832.
848   https://doi.org/10.1029/1999JD900141

849 Kasibhatla, P., Sherwen, T., Evans, M. J., Carpenter, L. J., Reed, C., Alexander, B., et al. (2018).
850   Global impact of nitrate photolysis in sea-salt aerosol on NOx, OH, and O3 in the marine
851   boundary layer. *Atmospheric Chemistry and Physics*, *18*(15), 11185–11203.
852   https://doi.org/10.5194/acp-18-11185-2018

853 Kenagy, H. S., Sparks, T. L., Ebben, C. J., Wooldrige, P. J., Lopez-Hilfiker, F. D., Lee, B. H., et
854   al. (2018). NO x Lifetime and NO y Partitioning During WINTER. *Journal of Geophysical
855   Research: Atmospheres*, *123*(17), 9813–9827. https://doi.org/10.1029/2018JD028736

856 Kleffmann, J., Becker, K. H., Lackhoff, M., & Wiesen, P. (1999). Heterogeneous conversion of
857   NO2 on carbonaceous surfaces. *Physical Chemistry Chemical Physics*, *1*(24), 5443–5450.
858   https://doi.org/10.1039/a905545b

859 Lamsal, L. N., Martin, R. V., van Donkelaar, A., Steinbacher, M., Celarier, E. A., Bucsela, E., et
860   al. (2008). Ground-level nitrogen dioxide concentrations inferred from the satellite-borne
861   Ozone Monitoring Instrument. *Journal of Geophysical Research*, *113*(D16), D16308.
862   https://doi.org/10.1029/2007JD009235

863 Le, T., Wang, Y., Liu, L., Yang, J., Yung, Y. L., Li, G., & Seinfeld, J. H. (2020). Unexpected air
864   pollution with marked emission reductions during the COVID-19 outbreak in China.

865   *Science*, *369*(6504), 702–706. https://doi.org/10.1126/science.abb7431

866   Lelieveld, J., Evans, J. S., Fnais, M., Giannadaki, D., & Pozzer, A. (2015). The contribution of
867   outdoor air pollution sources to premature mortality on a global scale. *Nature*, *525*(7569),
868   367–371. https://doi.org/10.1038/nature15371

869   Leung, D. M., Shi, H., Zhao, B., Wang, J., Ding, E. M., Gu, Y., et al. (2020). Wintertime
870   Particulate Matter Decrease Buffered by Unfavorable Chemical Processes Despite
871   Emissions Reductions in China. *Geophysical Research Letters*, *47*(14).
872   https://doi.org/10.1029/2020GL087721

873   Li, H., Cheng, J., Zhang, Q., Zheng, B., Zhang, Y., Zheng, G., & He, K. (2019). Rapid transition
874   in winter aerosol composition in Beijing from 2014 to 2017: response to clean air actions.
875   *Atmospheric Chemistry and Physics*, *19*(17), 11485–11499. https://doi.org/10.5194/acp-19-
876   11485-2019

877   Li, J., Chen, X., Wang, Z., Du, H., Yang, W., Sun, Y., et al. (2018). Radiative and heterogeneous
878   chemical effects of aerosols on ozone and inorganic aerosols over East Asia. *Science of the
879   Total Environment*, *622–623*, 1327–1342. https://doi.org/10.1016/j.scitotenv.2017.12.041

880   Li, K., Jacob, D. J., Liao, H., Zhu, J., Shah, V., Shen, L., et al. (2019). A two-pollutant strategy
881   for improving ozone and particulate air quality in China. *Nature Geoscience*, *12*(11), 906–
882   910. https://doi.org/10.1038/s41561-019-0464-x

883   Li, K., Jacob, D. J., Liao, H., Shen, L., Zhang, Q., & Bates, K. H. (2019). Anthropogenic drivers
884   of 2013-2017 trends in summer surface ozone in China. *Proceedings of the National
885   Academy of Sciences of the United States of America*, *116*(2), 422–427.
886   https://doi.org/10.1073/pnas.1812168116

887   Li, L., Hoffmann, M. R., & Colussi, A. J. (2018). Role of Nitrogen Dioxide in the Production of
888   Sulfate during Chinese Haze-Aerosol Episodes. *Environmental Science & Technology*,
889   *52*(5), 2686–2693. https://doi.org/10.1021/acs.est.7b05222

890   Li, M., Zhang, Q., Kurokawa, J., Woo, J.-H., He, K., Lu, Z., et al. (2017). MIX: a mosaic Asian
891   anthropogenic emission inventory under the international collaboration framework of the
892   MICS-Asia and HTAP. *Atmospheric Chemistry and Physics*, *17*(2), 935–963.
893   https://doi.org/10.5194/acp-17-935-2017

894   Lin, J. T., & McElroy, M. B. (2010). Impacts of boundary layer mixing on pollutant vertical
895   profiles in the lower troposphere: Implications to satellite remote sensing. *Atmospheric
896   Environment*, *44*(14), 1726–1739. https://doi.org/10.1016/j.atmosenv.2010.02.009

897   Liu, C., Ma, Z., Mu, Y., Liu, J., Zhang, C., Zhang, Y., et al. (2017). The levels, variation
898   characteristics, and sources of atmospheric non-methane hydrocarbon compounds during
899   wintertime in Beijing, China. *Atmospheric Chemistry and Physics*, *17*(17), 10633–10649.
900   https://doi.org/10.5194/acp-17-10633-2017

901   Liu, H., Jacob, D. J., Bey, I., & Yantosca, R. M. (2001). Constraints from 210 Pb and 7 Be on
902   wet deposition and transport in a global three-dimensional chemical tracer model driven by
903   assimilated meteorological fields. *Journal of Geophysical Research: Atmospheres*,
904   *106*(D11), 12109–12128. https://doi.org/10.1029/2000JD900839

905   Liu, P., Ye, C., Xue, C., Zhang, C., Mu, Y., & Sun, X. (2020). Formation mechanisms of

906   atmospheric nitrate and sulfate during the winter haze pollution periods in Beijing: gas-
907   phase, heterogeneous and aqueous-phase chemistry. *Atmospheric Chemistry and Physics*,
908   *20*(7), 4153–4165. https://doi.org/10.5194/acp-20-4153-2020

909   Liu, Y., Lu, K., Li, X., Dong, H., Tan, Z., Wang, H., et al. (2019). A Comprehensive Model Test
910   of the HONO Sources Constrained to Field Measurements at Rural North China Plain.
911   *Environmental Science & Technology*, *53*(7), 3517–3525.
912   https://doi.org/10.1021/acs.est.8b06367

913   Lu, K., Fuchs, H., Hofzumahaus, A., Tan, Z., Wang, H., Zhang, L., et al. (2019). Fast
914   Photochemistry in Wintertime Haze: Consequences for Pollution Mitigation Strategies.
915   *Environmental Science & Technology*, *53*(18), 10676–10684.
916   https://doi.org/10.1021/acs.est.9b02422

917   Mao, J., Fan, S., Jacob, D. J., & Travis, K. R. (2013). Radical loss in the atmosphere from Cu-Fe
918   redox coupling in aerosols. *Atmospheric Chemistry and Physics*, *13*(2), 509–519.
919   https://doi.org/10.5194/acp-13-509-2013

920   Marais, E. A., & Wiedinmyer, C. (2016). Air Quality Impact of Diffuse and Inefficient
921   Combustion Emissions in Africa (DICE-Africa). *Environmental Science & Technology*,
922   *50*(19), 10739–10745. https://doi.org/10.1021/acs.est.6b02602

923   McDonald, B. C., De Gouw, J. A., Gilman, J. B., Jathar, S. H., Akherati, A., Cappa, C. D., et al.
924   (2018). Volatile chemical products emerging as largest petrochemical source of urban
925   organic emissions. *Science*, *359*(6377), 760–764. https://doi.org/10.1126/science.aaq0524

926   McDuffie, E. E., Fibiger, D. L., Dubé, W. P., Lopez-Hilfiker, F., Lee, B. H., Thornton, J. A., et
927   al. (2018). Heterogeneous N2O5 Uptake During Winter: Aircraft Measurements During the
928   2015 WINTER Campaign and Critical Evaluation of Current Parameterizations. *Journal of
929   Geophysical Research: Atmospheres*, *123*(8), 4345–4372.
930   https://doi.org/10.1002/2018JD028336

931   Michalski, G., Scott, Z., Kabiling, M., & Thiemens, M. H. (2003). First measurements and
932   modeling of Δ 17 O in atmospheric nitrate. *Geophysical Research Letters*, *30*(16).
933   https://doi.org/10.1029/2003GL017015

934   Morin, S., Sander, R., & Savarino, J. (2011). Simulation of the diurnal variations of the oxygen
935   isotope anomaly (Δ17O) of reactive atmospheric species. *Atmospheric Chemistry and
936   Physics*, *11*(8), 3653–3671. https://doi.org/10.5194/acp-11-3653-2011

937   Murray, L. T., Jacob, D. J., Logan, J. A., Hudman, R. C., & Koshak, W. J. (2012). Optimized
938   regional and interannual variability of lightning in a global chemical transport model
939   constrained by LIS/OTD satellite data. *Journal of Geophysical Research: Atmospheres*,
940   *117*(D20). https://doi.org/10.1029/2012JD017934

941   Neu, J. L., Prather, M. J., & Penner, J. E. (2007). Global atmospheric chemistry: Integrating over
942   fractional cloud cover. *Journal of Geophysical Research*, *112*(D11), D11306.
943   https://doi.org/10.1029/2006JD008007

944   Reed, C., Evans, M. J., Di Carlo, P., Lee, J. D., & Carpenter, L. J. (2016). Interferences in
945   photolytic NO&lt;sub&gt;2&lt;/sub&gt; measurements: explanation for
946   an apparent missing oxidant? *Atmospheric Chemistry and Physics*, *16*(7), 4707–4724.
947   https://doi.org/10.5194/acp-16-4707-2016

948 Savarino, J., Morin, S., Erbland, J., Grannec, F., Patey, M. D., Vicars, W., et al. (2013). Isotopic
949   composition of atmospheric nitrate in a tropical marine boundary layer. *Proceedings of the*
950   *National Academy of Sciences*, *110*(44), 17668–17673.
951   https://doi.org/10.1073/pnas.1216639110

952 Shah, V., Jaeglé, L., Thornton, J. A., Lopez-Hilfiker, F. D., Lee, B. H., Schroder, J. C., et al.
953   (2018). Chemical feedbacks weaken the wintertime response of particulate sulfate and
954   nitrate to emissions reductions over the eastern United States. *Proceedings of the National*
955   *Academy of Sciences of the United States of America*, *115*(32), 8110–8115.
956   https://doi.org/10.1073/pnas.1803295115

957 Shah, V., Jacob, D. J., Li, K., Silvern, R. F., Zhai, S., Liu, M., et al. (2020). Effect of changing
958   NOx lifetime on the seasonality and long-term trends of satellite-observed tropospheric
959   NO2 columns over China. *Atmospheric Chemistry and Physics*, *20*(3), 1483–1495.
960   https://doi.org/10.5194/acp-20-1483-2020

961 Shao, J., Chen, Q., Wang, Y., Lu, X., He, P., Sun, Y., et al. (2019). Heterogeneous sulfate
962   aerosol formation mechanisms during wintertime Chinese haze events: air quality model
963   assessment using observations of sulfate oxygen isotopes in Beijing. *Atmospheric*
964   *Chemistry and Physics*, *19*(9), 6107–6123. https://doi.org/10.5194/acp-19-6107-2019

965 Sheng, J., Zhao, D., Ding, D., Li, X., Huang, M., Gao, Y., et al. (2018). Characterizing the level,
966   photochemical reactivity, emission, and source contribution of the volatile organic
967   compounds based on PTR-TOF-MS during winter haze period in Beijing, China.
968   *Atmospheric Research*, *212*, 54–63. https://doi.org/10.1016/j.atmosres.2018.05.005

969 Sherwen, T., Evans, M. J., Sommariva, R., Hollis, L. D. J., Ball, S. M., Monks, P. S., et al.
970   (2017). Effects of halogens on European air-quality. *Faraday Discussions*, *200*, 75–100.
971   https://doi.org/10.1039/C7FD00026J

972 Shi, G., Xu, J., Shi, X., Liu, B., Bi, X., Xiao, Z., et al. (2019). Aerosol pH Dynamics During
973   Haze Periods in an Urban Environment in China: Use of Detailed, Hourly, Speciated
974   Observations to Study the Role of Ammonia Availability and Secondary Aerosol Formation
975   and Urban Environment. *Journal of Geophysical Research: Atmospheres*, *124*(16), 9730–
976   9742. https://doi.org/10.1029/2018JD029976

977 Song, C., He, J., Wu, L., Jin, T., Chen, X., Li, R., et al. (2017). Health burden attributable to
978   ambient PM2.5 in China. *Environmental Pollution*, *223*, 575–586.
979   https://doi.org/10.1016/J.ENVPOL.2017.01.060

980 Song, W., Liu, X.-Y., Wang, Y.-L., Tong, Y.-D., Bai, Z.-P., & Liu, C.-Q. (2020). Nitrogen
981   isotope differences between atmospheric nitrate and corresponding nitrogen oxides: A new
982   constraint using oxygen isotopes. *Science of The Total Environment*, *701*, 134515.
983   https://doi.org/10.1016/j.scitotenv.2019.134515

984 Sun, J., Wang, Y., Wu, F., Tang, G., Wang, L., Wang, Y., & Yang, Y. (2018). Vertical
985   characteristics of VOCs in the lower troposphere over the North China Plain during
986   pollution periods. *Environmental Pollution*, *236*, 907–915.
987   https://doi.org/10.1016/j.envpol.2017.10.051

988 Sun, Y., Lei, L., Zhou, W., Chen, C., He, Y., Sun, J., et al. (2020). A chemical cocktail during
989   the COVID-19 outbreak in Beijing, China: Insights from six-year aerosol particle

990   composition measurements during the Chinese New Year holiday. *Science of the Total*
991   *Environment*, *742*, 140739. https://doi.org/10.1016/j.scitotenv.2020.140739

992 Tan, F., Tong, S., Jing, B., Hou, S., Liu, Q., Li, K., et al. (2016). Heterogeneous reactions of NO
993   2 with CaCO 3 –(NH 4) 2 SO 4 mixtures at different relative humidities. *Atmospheric*
994   *Chemistry and Physics*, *16*(13), 8081–8093. https://doi.org/10.5194/acp-16-8081-2016

995 Tan, F., Jing, B., Tong, S., & Ge, M. (2017). The effects of coexisting Na2SO4 on heterogeneous
996   uptake of NO2 on CaCO3 particles at various RHs. *Science of the Total Environment*, *586*,
997   930–938. https://doi.org/10.1016/j.scitotenv.2017.02.072

998 Tan, Z., Lu, K., Jiang, M., Su, R., Wang, H., Lou, S., et al. (2019). Daytime atmospheric
999   oxidation capacity in four Chinese megacities during the photochemically polluted season: a
1000   case study based on box model simulation. *Atmospheric Chemistry and Physics*, *19*(6),
1001   3493–3513. https://doi.org/10.5194/acp-19-3493-2019

1002 Tham, Y. J., Wang, Z., Li, Q., Yun, H., Wang, W., Wang, X., et al. (2016). Significant
1003   concentrations of nitryl chloride sustained in the morning: investigations of the causes and
1004   impacts on ozone production in a polluted region of northern China. *Atmospheric Chemistry*
1005   *and Physics*, *16*(23), 14959–14977. https://doi.org/10.5194/acp-16-14959-2016

1006 Thornton, J., & Abbatt, J. P. D. (2005). Measurements of HO 2 uptake to aqueous aerosol: Mass
1007   accommodation coefficients and net reactive loss. *Journal of Geophysical Research*,
1008   *110*(D8), D08309. https://doi.org/10.1029/2004JD005402

1009 Vicars, W. C., & Savarino, J. (2014). Quantitative constraints on the 17O-excess (Δ17O)
1010   signature of surface ozone: Ambient measurements from 50°N to 50°S using the nitrite-
1011   coated filter technique. *Geochimica et Cosmochimica Acta*, *135*, 270–287.
1012   https://doi.org/10.1016/j.gca.2014.03.023

1013 Wang, Jiaqi, Zhang, X., Guo, J., Wang, Z., & Zhang, M. (2017). Observation of nitrous acid
1014   (HONO) in Beijing, China: Seasonal variation, nocturnal formation and daytime budget.
1015   *Science of The Total Environment*, *587–588*, 350–359.
1016   https://doi.org/10.1016/j.scitotenv.2017.02.159

1017 Wang, Junfeng, Li, J., Ye, J., Zhao, J., Wu, Y., Hu, J., et al. (2020). Fast sulfate formation from
1018   oxidation of SO2 by NO2 and HONO observed in Beijing haze. *Nature Communications*,
1019   *11*(1), 2844. https://doi.org/10.1038/s41467-020-16683-x

1020 Wang, W., Li, X., Shao, M., Hu, M., Zeng, L., Wu, Y., & Tan, T. (2019). The impact of aerosols
1021   on photolysis frequencies and ozone production in Beijing during the 4-year period 2012–
1022   2015. *Atmospheric Chemistry and Physics*, *19*(14), 9413–9429. https://doi.org/10.5194/acp-
1023   19-9413-2019

1024 Wang, X., Jacob, D. J., Eastham, S. D., Sulprizio, M. P., Zhu, L., Chen, Q., et al. (2019). The
1025   role of chlorine in global tropospheric chemistry. *Atmospheric Chemistry and Physics*,
1026   *19*(6), 3981–4003. https://doi.org/10.5194/acp-19-3981-2019

1027 Wang, X., Jacob, D. J., Fu, X., Wang, T., Le Breton, M., Hallquist, M., et al. (2020). Effects of
1028   anthropogenic chlorine on PM 2.5 and ozone air quality in China. *Environmental Science &*
1029   *Technology*, acs.est.0c02296. https://doi.org/10.1021/acs.est.0c02296

1030 Wang, Yan-Li, Song, W., Yang, W., Sun, X., Tong, Y., Wang, X., et al. (2019). Influences of

Atmospheric Pollution on the Contributions of Major Oxidation Pathways to PM 2.5 Nitrate Formation in Beijing. *Journal of Geophysical Research: Atmospheres*, *124*(7), 4174–4185. https://doi.org/10.1029/2019JD030284

Wang, Yuhang, Jacob, D. J., & Logan, J. A. (1998). Global simulation of tropospheric O3-NOx-hydrocarbon chemistry: 1. Model formulation. *Journal of Geophysical Research: Atmospheres*, *103*(D9), 10713–10725. https://doi.org/10.1029/98JD00158

van der Werf, G. R., Randerson, J. T., Giglio, L., van Leeuwen, T. T., Chen, Y., Rogers, B. M., et al. (2017). Global fire emissions estimates during 1997–2016. *Earth System Science Data*, *9*(2), 697–720. https://doi.org/10.5194/essd-9-697-2017

Womack, C. C., McDuffie, E. E., Edwards, P. M., Bares, R., Gouw, J. A., Docherty, K. S., et al. (2019). An Odd Oxygen Framework for Wintertime Ammonium Nitrate Aerosol Pollution in Urban Areas: NOx and VOC Control as Mitigation Strategies. *Geophysical Research Letters*, *46*(9), 4971–4979. https://doi.org/10.1029/2019GL082028

Xia, M., Wang, W., Wang, Z., Gao, J., Li, H., Liang, Y., et al. (2019). Heterogeneous uptake of N2O5 in sand dust and urban aerosols observed during the dry season in Beijing. *Atmosphere*, *10*(4), 204. https://doi.org/10.3390/ATMOS10040204

Xu, Q., Wang, S., Jiang, J., Bhattarai, N., Li, X., Chang, X., et al. (2019). Nitrate dominates the chemical composition of PM2.5 during haze event in Beijing, China. *Science of the Total Environment*, *689*, 1293–1303. https://doi.org/10.1016/j.scitotenv.2019.06.294

Yan, Y., Peng, L., Li, R., Li, Y., Li, L., & Bai, H. (2017). Concentration, ozone formation potential and source analysis of volatile organic compounds (VOCs) in a thermal power station centralized area: A study in Shuozhou, China. *Environmental Pollution*, *223*, 295–304. https://doi.org/10.1016/j.envpol.2017.01.026

Ye, C., Zhang, N., Gao, H., & Zhou, X. (2017). Photolysis of Particulate Nitrate as a Source of HONO and NOx. *Environmental Science & Technology*, *51*(12), 6849–6856. https://doi.org/10.1021/acs.est.7b00387

Yu, C., Wang, Z., Xia, M., Fu, X., Wang, W., Tham, Y. J., et al. (2020). Heterogeneous N2O5 reactions on atmospheric aerosols at four Chinese sites: improving model representation of uptake parameters. *Atmospheric Chemistry and Physics*, *20*(7), 4367–4378. https://doi.org/10.5194/acp-20-4367-2020

Yu, D., Tan, Z., Lu, K., Ma, X., Li, X., Chen, S., et al. (2020). An explicit study of local ozone budget and NOx-VOCs sensitivity in Shenzhen China. *Atmospheric Environment*, *224*, 117304. https://doi.org/10.1016/j.atmosenv.2020.117304

Zhang, B., Zhao, B., Zuo, P., Huang, Z., & Zhang, J. (2017). Ambient peroxyacyl nitrate concentration and regional transportation in Beijing. *Atmospheric Environment*, *166*, 543–550. https://doi.org/10.1016/j.atmosenv.2017.07.053

Zhang, G., Xia, L., Zang, K., Xu, W., Zhang, F., Liang, L., et al. (2020). The abundance and inter-relationship of atmospheric peroxyacetyl nitrate (PAN), peroxypropionyl nitrate (PPN), O3, and NOy during the wintertime in Beijing, China. *Science of the Total Environment*, *718*, 137388. https://doi.org/10.1016/j.scitotenv.2020.137388

Zhang, H., Xu, X., Lin, W., & Wang, Y. (2014). Wintertime peroxyacetyl nitrate (PAN) in the

1072   megacity Beijing: Role of photochemical and meteorological processes. *Journal of*
1073   *Environmental Sciences (China)*, *26*(1), 83–96. https://doi.org/10.1016/S1001-
1074   0742(13)60384-8

1075 Zhang, J., An, J., Qu, Y., Liu, X., & Chen, Y. (2019). Impacts of potential HONO sources on the
1076   concentrations of oxidants and secondary organic aerosols in the Beijing-Tianjin-Hebei
1077   region of China. *Science of The Total Environment*, *647*, 836–852.
1078   https://doi.org/10.1016/j.scitotenv.2018.08.030

1079 Zhang, L., Gong, S., Padro, J., & Barrie, L. (2001). A size-segregated particle dry deposition
1080   scheme for an atmospheric aerosol module. *Atmospheric Environment*, *35*(3), 549–560.
1081   https://doi.org/10.1016/S1352-2310(00)00326-5

1082 Zhang, Y.-L., & Cao, F. (2015). Fine particulate matter (PM2.5) in China at a city level.
1083   *Scientific Reports*, *5*(1), 14884. https://doi.org/10.1038/srep14884

1084 Zheng, B., Tong, D., Li, M., Liu, F., Hong, C., Geng, G., et al. (2018). Trends in China's
1085   anthropogenic emissions since 2010 as the consequence of clean air actions. *Atmospheric*
1086   *Chemistry and Physics*, *18*(19), 14095–14111. https://doi.org/10.5194/acp-18-14095-2018

1087 Zhou, W., Zhao, J., Ouyang, B., Mehra, A., Xu, W., Wang, Y., et al. (2018). Production of N2O5
1088   and ClNO2 in summer in urban Beijing, China. *Atmospheric Chemistry and Physics*,
1089   *18*(16), 11581–11597. https://doi.org/10.5194/acp-18-11581-2018

1090 Zhou, W., Gao, M., He, Y., Wang, Q., Xie, C., Xu, W., et al. (2019). Response of aerosol
1091   chemistry to clean air action in Beijing, China: Insights from two-year ACSM
1092   measurements and model simulations. *Environmental Pollution*, *255*, 113345.
1093   https://doi.org/10.1016/j.envpol.2019.113345

1094

Other supporting references

Acton, W. J. F., Huang, Z., Davison, B., Drysdale, W. S., Fu, P., Hollaway, M., et al. (2020). Surface–atmosphere fluxes of volatile organic compounds in Beijing. *Atmospheric Chemistry and Physics*, *20*(23), 15101–15125. https://doi.org/10.5194/acp-20-15101-2020

Fu, X., Wang, T., Zhang, L., Li, Q., Wang, Z., Xia, M., et al. (2019). The significant contribution of HONO to secondary pollutants during a severe winter pollution event in southern China. *Atmospheric Chemistry and Physics*, *19*(1), 1–14. https://doi.org/10.5194/acp-19-1-2019

Haskins, J. D., Lopez-Hilfiker, F. D., Lee, B. H., Shah, V., Wolfe, G. M., DiGangi, J., et al. (2019). Anthropogenic Control Over Wintertime Oxidation of Atmospheric Pollutants. *Geophysical Research Letters*, *46*(24), 14826–14835. https://doi.org/10.1029/2019GL085498

Hoffmann, E. H., Tilgner, A., Vogelsberg, U., Wolke, R., & Herrmann, H. (2019). Near-Explicit Multiphase Modeling of Halogen Chemistry in a Mixed Urban and Maritime Coastal Area. *ACS Earth and Space Chemistry*, *3*(11), 2452–2471. https://doi.org/10.1021/acsearthspacechem.9b00184

Li, D., Xue, L., Wen, L., Wang, X., Chen, T., Mellouki, A., et al. (2018). Characteristics and sources of nitrous acid in an urban atmosphere of northern China: Results from 1-yr continuous observations. *Atmospheric Environment*, *182*, 296–306. https://doi.org/10.1016/J.ATMOSENV.2018.03.033

Li, J., Xie, S. D., Zeng, L. M., Li, L. Y., Li, Y. Q., & Wu, R. R. (2015). Characterization of ambient volatile organic compounds and their sources in Beijing, before, during, and after Asia-Pacific Economic Cooperation China 2014. *Atmospheric Chemistry and Physics*, *15*(14), 7945–7959. https://doi.org/10.5194/acp-15-7945-2015

Li, K., Li, J., Tong, S., Wang, W., Huang, R.-J., & Ge, M. (2019). Characteristics of wintertime VOCs in suburban and urban Beijing: concentrations, emission ratios, and festival effects. *Atmospheric Chemistry and Physics*, *19*(12), 8021–8036. https://doi.org/10.5194/acp-19-8021-2019

Li, Q., Badia, A., Wang, T., Sarwar, G., Fu, X., Zhang, L., et al. (2020). Potential Effect of Halogens on Atmospheric Oxidation and Air Quality in China. *Journal of Geophysical Research: Atmospheres*, *125*(9). https://doi.org/10.1029/2019JD032058

McCulloch, A., Aucott, M. L., Benkovitz, C. M., Graedel, T. E., Kleiman, G., Midgley, P. M., & Li, Y.-F. (1999). Global emissions of hydrogen chloride and chloromethane from coal combustion, incineration and industrial activities: Reactive Chlorine Emissions Inventory. *Journal of Geophysical Research: Atmospheres*, *104*(D7), 8391–8403. https://doi.org/10.1029/1999JD900025

Romer, P. S., Wooldridge, P. J., Crounse, J. D., Kim, M. J., Wennberg, P. O., Dibb, J. E., et al. (2018). Constraints on Aerosol Nitrate Photolysis as a Potential Source of HONO and NO x. *Environmental Science & Technology*, *52*(23), 13738–13746. https://doi.org/10.1021/acs.est.8b03861

Shi, Y., Hu, F., Xiao, Z., Fan, G., & Zhang, Z. (2020). Comparison of four different types of planetary boundary layer heights during a haze episode in Beijing. *Science of the Total Environment*, *711*, 134928. https://doi.org/10.1016/j.scitotenv.2019.134928

1137　Su, T., Li, Z., & Kahn, R. (2018). Relationships between the planetary boundary layer height and
1138　　　surface pollutants derived from lidar observations over China: regional pattern and
1139　　　influencing factors. *Atmospheric Chemistry and Physics*, *18*(21), 15921–15935.
1140　　　https://doi.org/10.5194/acp-18-15921-2018

1141　Tang, G., Zhang, J., Zhu, X., Song, T., Münkel, C., Hu, B., et al. (2016). Mixing layer height and
1142　　　its implications for air pollution over Beijing, China. *Atmospheric Chemistry and Physics*,
1143　　　*16*(4), 2459–2475. https://doi.org/10.5194/acp-16-2459-2016

1144

1145
1146

References From the Supporting Information

Acton, W. J. F., Huang, Z., Davison, B., Drysdale, W. S., Fu, P., Hollaway, M., et al. (2020). Surface–atmosphere fluxes of volatile organic compounds in Beijing. *Atmospheric Chemistry and Physics*, *20*(23), 15101–15125. https://doi.org/10.5194/acp-20-15101-2020

Fu, X., Wang, T., Zhang, L., Li, Q., Wang, Z., Xia, M., et al. (2019). The significant contribution of HONO to secondary pollutants during a severe winter pollution event in southern China. *Atmospheric Chemistry and Physics*, *19*(1), 1–14. https://doi.org/10.5194/acp-19-1-2019

Haskins, J. D., Lopez-Hilfiker, F. D., Lee, B. H., Shah, V., Wolfe, G. M., DiGangi, J., et al. (2019). Anthropogenic Control Over Wintertime Oxidation of Atmospheric Pollutants. *Geophysical Research Letters*, *46*(24), 14826–14835. https://doi.org/10.1029/2019GL085498

Hoffmann, E. H., Tilgner, A., Vogelsberg, U., Wolke, R., & Herrmann, H. (2019). Near-Explicit Multiphase Modeling of Halogen Chemistry in a Mixed Urban and Maritime Coastal Area. *ACS Earth and Space Chemistry*, *3*(11), 2452–2471. https://doi.org/10.1021/acsearthspacechem.9b00184

Li, D., Xue, L., Wen, L., Wang, X., Chen, T., Mellouki, A., et al. (2018). Characteristics and sources of nitrous acid in an urban atmosphere of northern China: Results from 1-yr continuous observations. *Atmospheric Environment*, *182*, 296–306. https://doi.org/10.1016/J.ATMOSENV.2018.03.033

Li, J., Xie, S. D., Zeng, L. M., Li, L. Y., Li, Y. Q., & Wu, R. R. (2015). Characterization of ambient volatile organic compounds and their sources in Beijing, before, during, and after Asia-Pacific Economic Cooperation China 2014. *Atmospheric Chemistry and Physics*, *15*(14), 7945–7959. https://doi.org/10.5194/acp-15-7945-2015

Li, K., Li, J., Tong, S., Wang, W., Huang, R.-J., & Ge, M. (2019). Characteristics of wintertime VOCs in suburban and urban Beijing: concentrations, emission ratios, and festival effects. *Atmospheric Chemistry and Physics*, *19*(12), 8021–8036. https://doi.org/10.5194/acp-19-8021-2019

Li, Q., Badia, A., Wang, T., Sarwar, G., Fu, X., Zhang, L., et al. (2020). Potential Effect of Halogens on Atmospheric Oxidation and Air Quality in China. *Journal of Geophysical Research: Atmospheres*, *125*(9). https://doi.org/10.1029/2019JD032058

McCulloch, A., Aucott, M. L., Benkovitz, C. M., Graedel, T. E., Kleiman, G., Midgley, P. M., & Li, Y.-F. (1999). Global emissions of hydrogen chloride and chloromethane from coal combustion, incineration and industrial activities: Reactive Chlorine Emissions Inventory. *Journal of Geophysical Research: Atmospheres*, *104*(D7), 8391–8403. https://doi.org/10.1029/1999JD900025

Romer, P. S., Wooldridge, P. J., Crounse, J. D., Kim, M. J., Wennberg, P. O., Dibb, J. E., et al. (2018). Constraints on Aerosol Nitrate Photolysis as a Potential Source of HONO and NO x. *Environmental Science & Technology*, *52*(23), 13738–13746. https://doi.org/10.1021/acs.est.8b03861

Shi, Y., Hu, F., Xiao, Z., Fan, G., & Zhang, Z. (2020). Comparison of four different types of planetary boundary layer heights during a haze episode in Beijing. *Science of the Total*

1189   *Environment*, *711*, 134928. https://doi.org/10.1016/j.scitotenv.2019.134928

1190 Su, T., Li, Z., & Kahn, R. (2018). Relationships between the planetary boundary layer height and
1191   surface pollutants derived from lidar observations over China: regional pattern and
1192   influencing factors. *Atmospheric Chemistry and Physics*, *18*(21), 15921–15935.
1193   https://doi.org/10.5194/acp-18-15921-2018

1194 Tang, G., Zhang, J., Zhu, X., Song, T., Münkel, C., Hu, B., et al. (2016). Mixing layer height and
1195   its implications for air pollution over Beijing, China. *Atmospheric Chemistry and Physics*,
1196   *16*(4), 2459–2475. https://doi.org/10.5194/acp-16-2459-2016
1197
1198